


Selective Deletion of Methyl CpG Binding Protein 2 from Parvalbumin Interneurons in the Auditory Cortex Delays the Onset of Maternal Retrieval in Mice

Deborah D. Rupert,^{1,2} Alexa H. Pagliaro,² Jane Choe,² and  Stephen D. Shea²

¹Department of Neurobiology and Behavior and Medical Scientist Training Program, School of Medicine, Stony Brook University, Stony Brook, New York 11794-8434 and ²Cold Spring Harbor Laboratory, Cold Spring Harbor, New York 11724

Mutations in *MECP2* cause the neurodevelopmental disorder Rett syndrome. *MECP2* codes for methyl CpG binding protein 2 (MECP2), a transcriptional regulator that activates genetic programs for experience-dependent plasticity. Many neural and behavioral symptoms of Rett syndrome may result from dysregulated timing and thresholds for plasticity. As a model of adult plasticity, we examine changes to auditory cortex inhibitory circuits in female mice when they are first exposed to pups; this plasticity facilitates behavioral responses to pups emitting distress calls. Brainwide deletion of *Mecp2* alters expression of markers associated with GABAergic parvalbumin interneurons (PVins) and impairs the emergence of pup retrieval. We hypothesized that loss of *Mecp2* in PVins disproportionately contributes to the phenotype. Here, we find that deletion of *Mecp2* from PVins delayed the onset of maternal retrieval behavior and recapitulated the major molecular and neurophysiological features of brainwide deletion of *Mecp2*. We observed that when PVin-selective mutants were exposed to pups, auditory cortical expression of PVin markers increased relative to that in wild-type littermates. PVin-specific mutants also failed to show the inhibitory auditory cortex plasticity seen in wild-type mice on exposure to pups and their vocalizations. Finally, using an intersectional viral genetic strategy, we demonstrate that postdevelopmental loss of *Mecp2* in PVins of the auditory cortex is sufficient to delay onset of maternal retrieval. Our results support a model in which PVins play a central role in adult cortical plasticity and may be particularly impaired by loss of *Mecp2*.

Key words: auditory cortex; inhibition; maternal behavior; *Mecp2*; parvalbumin; plasticity

Significance Statement

Rett syndrome is a neurodevelopmental disorder that includes deficits in both communication and the ability to update brain connections and activity during learning (plasticity). This condition is caused by mutations in the gene *MECP2*. We use a maternal behavioral test in mice requiring both vocal perception and neural plasticity to probe the role of *Mecp2* in social and sensory learning. *Mecp2* is normally active in all brain cells, but here we remove it from a specific population (parvalbumin neurons). We find that this is sufficient to delay learned behavioral responses to pups and recreates many deficits seen in whole-brain *Mecp2* deletion. Our findings suggest that parvalbumin neurons specifically are central to the consequences of loss of *Mecp2* activity and yield clues as to possible mechanisms by which Rett syndrome impairs brain function.

Received May 8, 2023; revised Aug. 5, 2023; accepted Aug. 15, 2023.

Author contributions: D.D.R., A.H.P., J.C., and S.D.S. designed research; D.D.R., A.H.P., J.C., and S.D.S. performed research; D.D.R., A.H.P., J.C., and S.D.S. analyzed data; and D.D.R., A.H.P., and S.D.S. wrote the paper.

This work was supported by National Institutes of Health—National Institute of Mental Health Grant R01MH106656 and a Feil Foundation grant to S.D.S. and an Autism Speaks Royal Arch Masons Predoctoral Fellowship (#11001) to D.D.R. We thank A. Zador, H. Hsieh, Z. J. Huang, and A. Banerjee for comments and guidance; C. Nguyen, C. Kelahan, and R. Palaniswamy for technical support; and Rob Eifert and the Cold Spring Harbor Laboratory machine shop staff for equipment support.

The authors declare no competing financial interests.

Correspondence should be addressed to Stephen D. Shea at sshea@cshl.edu.

<https://doi.org/10.1523/JNEUROSCI.0838-23.2023>

Copyright © 2023 the authors

Introduction

Rett syndrome (RTT) is a pervasive neurodevelopmental disorder that results from sporadic, *de novo* loss-of-function mutations in the *MECP2* gene, which codes for the transcriptional regulator methyl CpG binding protein-2 (Amir et al., 1999; Samaco et al., 2008). Because *MECP2* is located on the X chromosome, when it possesses a disabling mutation, males (or other individuals with a single X chromosome) lose their sole functioning copy and typically die perinatally; females (or other individuals with two X chromosomes) have heterozygous mosaic expression and frequently survive infancy with impairments in cognition, musculoskeletal structure, metabolism (Van den Veyver and Zoghbi, 2000; Braunschweig et al., 2004), auditory processing, language, and

communication (Bashina et al., 2002; Glaze, 2005). *MECP2* has been repeatedly implicated in the regulation of neural plasticity (Deng et al., 2010; McGraw et al., 2011; Noutel et al., 2011; Na et al., 2013; Deng et al., 2014; He et al., 2014; Krishnan et al., 2015; Tai et al., 2016; Krishnan et al., 2017; Gulmez Karaca et al., 2018). This observation, combined with the nonlinear developmental course of RTT, has fueled speculation that *MECP2* is most essential during periods of elevated neuronal plasticity, for example, early critical periods (He et al., 2014; Krishnan et al., 2015).

Mouse models in which *Mecp2* expression has either been disabled (Chen et al., 2001; Guy et al., 2001) or deleted with spatiotemporal selectivity using flanking loxP sites and cell-type-specific expression of Cre recombinase (Gemelli et al., 2006) have been invaluable for understanding the biology of *Mecp2*. We capitalize on these models with a natural behavior, pup retrieval by female mice, as a readout of cortical plasticity and function (Krishnan et al., 2017; Lau et al., 2020). Our past work was performed in female mice that lacked one functional copy of *Mecp2* (*Mecp2*^{het}). The mosaicism in these mice more closely represents the genetic condition in humans, compared with the more commonly used male null model.

When female mice are exposed to pups, they become primed to exhibit pup retrieval (Rosenblatt, 1967; Sewell, 1970; Ehret et al., 1987), a learned behavioral response to the ultrasonic cries emitted by distressed or wandering pups (Galindo-Leon et al., 2009; Cohen et al., 2011; Cohen and Mizrahi, 2015; Lau et al., 2020; Carcea et al., 2021). Most wild-type females subsequently rapidly increase the speed of retrieval over the first day or two. Emergence of retrieval in adult females is accompanied by changes in the inhibitory circuitry of the auditory cortex (Liu and Schreiner, 2007; Galindo-Leon et al., 2009; Cohen et al., 2011; Lin et al., 2013; Cohen and Mizrahi, 2015; Marlin et al., 2015; Lau et al., 2020). *Mecp2* expression is specifically required in the auditory cortex at the time of pup exposure for proper retrieval (Krishnan et al., 2017). Moreover, loss of *Mecp2* triggers overexpression of parvalbumin (PV) and the extracellular matrix structures perineuronal nets (PNNs) (Krishnan et al., 2017). These two markers associated with the PVins are thought to act as brakes on cortical plasticity (Krishnan et al., 2017). Restoration of normal levels of PV and PNN expression in the auditory cortex improved behavior and restored physiological plasticity (Krishnan et al., 2017; Lau et al., 2020). Given that changes in PVin-specific markers were correlated with retrieval behavior performance, we speculated that PVins are central to the behavioral phenotype of *Mecp2*^{het}.

Loss of *Mecp2* appears to be more detrimental in certain cell types. For example, inhibitory cells may be particularly impaired by loss of *Mecp2*. Restriction of *Mecp2* mutation to either all GABAergic cells or to selected inhibitory subclasses (e.g., parvalbumin- or somatostatin-positive interneurons) is sufficient for recapitulating the majority of phenotypes in mouse models (Chao et al., 2010; He et al., 2014; Ito-Ishida et al., 2015; Mossner et al., 2020). Other work has demonstrated selected behavioral effects resulting from loss of *Mecp2* in excitatory neurons (Chao et al., 2007; Meng et al., 2016). Here, we use cell-type-specific removal of *Mecp2* and show that PVins are the only major class of interneurons that significantly affect retrieval when depleted of *Mecp2*. Mice of the genotype *PV-Cre*⁺/*Mecp2*^{lox} (hereafter, *PV-Mecp2* mutants), which lack *Mecp2* in all PVin, are delayed in the onset of pup retrieval and recapitulate all the major features of *Mecp2*^{het}. Specifically, when virgin *PV-Mecp2* mutant females were exposed to pups, they exhibited elevated expression of PV and PNNs relative to *Mecp2*^{wt}. PVin-specific mutants also did

not show the experience-dependent disinhibition of auditory cortex seen in *Mecp2*^{wt} controls. Finally, deleting PVins in the auditory cortex in adulthood was sufficient to delay pup retrieval. Together, these findings are consistent with the conclusion that *Mecp2* in auditory cortex PVins is critical for initiating experience-dependent auditory plasticity that facilitates the emergence of maternal retrieval.

Materials and Methods

Animals

All procedures were conducted in accordance with the National Institutes of Health *Guide for the Care and Use of Laboratory Animals* and approved by the Cold Spring Harbor Laboratory Institutional Animal Care and Use Committee. Animals were maintained on a 12 h light/dark cycle and received food and water *ad libitum*. Behavioral experiments were conducted during light-cycle hours.

Subjects were adult, female mice 6–12 weeks of age, bred in house from founders obtained from The Jackson Laboratory or the Mutant Mouse Resource and Research Center (MMRRC). The following genotypes were used: CBA/CaJ, B6.129P2(C)-*Mecp2*^{tm1.1Bird/J} (*Mecp2*^{het}; catalog #003890, The Jackson Laboratory), B6.129S4-*Mecp2*^{tm1Jae/Mmucd} (*Mecp2*^{lox}; catalog #011918, MMRRC), B6.129P2-Pvalb^{tm1(Cre)Arbr/J} (PV-Cre; catalog #017320, The Jackson Laboratory), *Vip*^{tm(Cre)zjh/J} (VIP-Cre; catalog #010908, The Jackson Laboratory), *Sst*^{tm2.1(Cre)zjh/J} (SST-Cre; catalog #013044, The Jackson Laboratory), B6.129S2^{tm(emx1)krj/J} (*Emx1-Cre*; catalog #005628, The Jackson Laboratory), and PV-Flp B6.Cg-Pvalb^{tm4.1(flopo)Hze/J} (PV-Flp; catalog #022730, The Jackson Laboratory). All crosses between Cre/Flp recombinase lines were established by pairing carriers of each allele such that all female test subject cagemates (controls and mutants) were homozygous for the *Mecp2*-lox allele and had 0–2 copies of the relevant recombinase allele. For example, in the PV-*Mecp2* line, PV-*Mecp2* mutants were either PV-ires-Cre^{+/-} or PV-ires-Cre^{+/+} and were homozygous for *Mecp2*^{lox} (*Mecp2*^{lox/lox}). PV-*Mecp2* wild-type (WT) controls were negative for the recombinase (PV-ires-Cre^{-/-}) but homozygous for *Mecp2*^{lox}.

All animals were genotyped at the time of weaning, ~3 weeks of age, according to standard protocols from the source. In some cases, genotyping was performed by an external service (Transnetyx) using their suggested probes or probes from The Jackson Laboratory. All lines were monitored for the possibility of somatic recombination affecting the *Mecp2* gene as per The Jackson Laboratory recommendations.

Behavioral analysis

Pup retrieval behavior was conducted as previously described (Krishnan et al., 2017) and aided by automated tracking with DeepLabCut software (Mathis et al., 2018). In brief, virgin adult female test subjects (surrogates) were cohoused with a WT (CBA) pregnant dam 2–5 d prepartum. Starting at postnatal day (P)0, subjects were tested daily for 3 consecutive days in a pup retrieval assay as follows. Pups were isolated for 2 min and then scattered to set positions in the home cage. Surrogates were allowed to interact with scattered pups for 5 min. Animals not currently performing the retrieval assay, including the dam, were temporarily placed in a group holding cage. Holding cages and home cages were not changed for the duration of retrieval experiments (i.e., from the time of surrogate pairing to P2). A normalized latency score between zero (instantaneous gathering of all pups) and one (failure to gather all pups) was calculated as follows:

$$\text{Latency} = \frac{\sum (t_1 - t_0) \dots (t_n - t_0)}{n * L},$$

where, n indicates the number of pups outside the nest, t_0 is start of trial, t_n is time of n th pup gathered, and L is trial length.

Surgeries and injections

All surgeries were performed on a Kopf stereotaxic device. Anesthesia induction was achieved with a bolus intraperitoneal injection of a

ketamine (100 mg/kg) and xylazine (5 mg/kg) mixture and maintained for long surgeries (>2 h) with inhaled isoflurane (1–2%) in oxygen (2–4 liters per min), adjusted as needed based on assessment of the depth of anesthesia with a tail/paw pinch every 30 min. At the end of surgery, a nonsteroidal anti-inflammatory (meloxicam, 2 mg/kg, i.p.) and an antibiotic (enrofloxacin, selected for its lack of ototoxicity, 4 mg/kg, i.p.) were administered for analgesia and infection prophylaxis.

All animals used for *in vivo* physiology or fiber photometry experiments had a custom titanium head bar affixed to the skull at the time of craniotomy. To optimize the stability of the head bar, the surface of the skull was lightly, manually etched with a scalpel, and three different dental cements were applied, Metabond Quick (C&B), Vitrebond Light Cure Glass Ionomer (3M), and Ortho-Jet (Lang Dental). Mice used for fiber photometric recordings were also fitted with optical fiber implants secured with dental cement. Uncleaved fibers (0.39 NA, 200 μ m diameter, 1.25 mm length) (catalog #CFMLC12U-20, Thorlabs) were manually cleaved to the desired length using a Ruby Scribe (catalog #S90R, Thorlabs). A guide (catalog #OGL-5, Thorlabs) was also secured (LOCTITE, Henkel Adhesives) into place, and the optical fiber implants were lowered into the auditory cortex to a depth of 700 μ m. Implants were allowed to cure >48 h before head fixation or attachment of an optical cable. Braided silk surgical sutures (CP Medical) and/or Vetbond tissue adhesive (3M) were used to close surgical sites around headgear.

Thalamorecipient core auditory cortex (Lin et al., 2013) was targeted for adeno-associated virus (AAV) injections and neurophysiology recordings using the following coordinates relative to bregma: anterior 2.5 mm (\pm 0.4 mm) and lateral 3.9 mm (\pm 0.3 mm). For AAV-injection experiments, 90 nl injections (delivered at 20 nl/min) were administered via glass pipettes (20 μ m tip) at six locations per hemisphere, relative to bregma (anterior 2.1 mm, 2.4 mm, and 2.7 mm at lateral 3.8 mm and 4.0 mm). Viruses used were pAAV-EF1a-fDIO-Cre (catalog #121675-AAV9, Addgene) or pAAV.Syn.Flex.GCaMP7s.WPRE.SV (catalog #104491-AAV9, Addgene).

Immunohistochemistry

Subjects were injected intraperitoneally with a lethal dose of Euthasol (pentobarbital sodium and phenytoin sodium cocktail) and transcardially perfused with ice-cold PBS followed by paraformaldehyde (PFA). Brains were extracted and fixed overnight in PFA at 4°C before being transferred to a 30% sucrose solution in PBS again at 4°C overnight or until buoyancy of the tissue was lost. Frozen 45 μ m sections were collected using a sliding microtome (Leica SM2010 R). Free-floating sections were preserved for batch immunohistochemical (IHC) staining in cryoprotectant solution at -20°C . Cryoprotectant solution consisted of sucrose (0.3 g/ml), polyvinyl-pyrrolidone (0.01 g/ml), and ethylene glycol (0.5 ml/ml) in 0.1 M PB.

For all staining protocols, free-floating sections were washed three times at room temperature (RT) in PBS and 0.3% Triton X-100, followed with a 30 min wash in 0.3% hydrogen peroxide solution to decrease non-specific background staining. Subsequently, sections were incubated in 5% normal goat or donkey serum, in accordance with the chosen secondary antibody, and then primary antibody solution at 4°C overnight. The following primary antibodies and dilutions were used to stain for *MeCP2*, parvalbumin, and perineuronal nets, respectively: rabbit anti-*MeCP2* (1:1000; Cell Signaling Technology), mouse anti-parvalbumin (1:1000; Sigma-Aldrich), and lectin from *Wisteria floribunda* with biotin conjugate (1:1000; Sigma-Aldrich). Rabbit anti-HA-Tag (1:500; Abcam) was used on alternating sections to detect cells expressing pAAV-EF1a-fDIO-Cre in PV-Flp subjects. In a subset of animals used for fiber photometry, staining was used to amplify *GCaMP* expression with chicken anti-GFP (1:1000; Aves Labs). Sections were washed three times at RT before transfer to secondary antibody solution. Primary antibody staining was visualized with the following Alexa Fluor conjugated secondary antibodies: goat AF 488, goat AF 594, and donkey AF 633 (Invitrogen Technologies). Secondary antibody dilutions matched those for the targeted primary antibody. Sections were exposed to secondary antibodies for 2 h at RT.

Imaging and quantification

A 20 \times magnification was used to collect *z*-stack images on a 710 confocal microscope (Zeiss) in line scan mode. The spectra for each channel

were manually adjusted to optimize signal-to-noise ratio using staining from a naive WT sample. Those settings were as follows: bit depth = 12; laser power = 10%; gain < 700, pinhole size lowest value for each channel; full dynamic range, 1024 \times 1024 pixel smoothness, averaging = 4. These settings were used to acquire all images across batches of a given stain. For each brain, six to eight matched sections spanning the rostral-caudal axis of the auditory cortex were selected for imaging. Maximum intensity projection images were generated for each field of view.

To quantify per-cell staining intensity, Fiji (ImageJ) software was used to manually outline cells and apply area-integrated intensity in the set measurements panel. Background intensity readings for each section were subtracted from the cell intensity values. Cells were counted using Fiji (ImageJ) software and normalized to the volume of auditory cortex represented in images based on the size of the image and the depth of the *z*-stacks ($\mu\text{m} \times \mu\text{m} \times \mu\text{m}$). Mean cell density was determined by averaging counts per volume across sections.

In vivo physiology

Loose-patch recordings from the auditory cortex were performed in awake, head-fixed subjects that were allowed to freely run on an axially rotating foam wheel as previously described (Cazakoff et al., 2014; Lau et al., 2020). Animals were habituated to head fixation and the wheel for 15–30 min/d for 1–2 d before recordings were collected. For each subject, a small craniotomy (200 \times 200 μm) was made over the auditory cortex. Subjects were head fixed by bolting the titanium bar implant to a frame suspended above a freely rotating foam wheel for the duration of the recording. Recordings were performed over 2–3 consecutive daily sessions (<8 h). Gelfoam (absorbable gelatin sponge, Ethicon) soaked in sterile saline was used to keep the surface of the cortex moist between recording periods during the session, and craniotomy sites were covered with Kwik-Cast between days of recording.

Single-unit recordings were made with a bridge amplifier (BA-03X, NPI). Borosilicate glass micropipettes (15–40 M Ω) were pulled on a horizontal pipette puller (model P-1000, Sutter Instrument). Pipettes were filled with an intracellular solution containing the following (in mM): 125 potassium gluconate, 10 potassium chloride, 2 magnesium chloride, and 10 HEPES. Single neurons were recorded blind by advancing the pipette in 3–5 μm steps using a single-axis stepper motor and controller (Solo, Sutter Instrument) or hydraulic micromanipulator (MX610, Siskiyou) as positive pressure was applied to the tip. Brief, small injected currents (-200 pA, 200 ms) were made at 2 Hz to monitor tip resistance, and the capacitance buzz feature on the amplifier was used to clear debris. Voltage signals were low-pass filtered (3 kHz), digitized (10 kHz), and acquired using Spike2 software and Cambridge Electronic Design hardware (Power1401). All cells were recorded at a depth <1 mm.

Auditory stimuli consisted of seven logarithmically spaced tones from 16 to 64 kHz and a library of eight ultrasonic vocalizations (USVs) recorded from WT CBA/CaJ mouse pups (2–4 d old) inside an anechoic isolation chamber (Industrial Acoustics) using an ultrasound microphone (Avisoft Bioacoustics) suspended 30 cm above the pup. Tone and call stimuli were played separately in a pseudorandom order with a 4 s interstimulus interval. Stimulus files that had been digitally sampled at 195.3 kHz were converted to analog output via Cambridge Electronic Design hardware (Power1401). Stimuli were low-pass filtered (100 kHz) and amplified with custom-built hardware (Kiwa Electronics) before being output through an electrostatic speaker and driver (ED1/ES1, Tucker-Davis Technologies) 4 inches directly in front of the animal. Speaker output was calibrated to 65 dB SPL at the head of the mouse with a sound level meter (model 407736, Extech) using A-weighting by comparing with an 8 kHz reference tone. The speaker had a relatively flat output (\pm 11 dB) at 4–100 kHz.

Fiber photometry

PV-Cre mice (WT, *Mecp2*^{fllox}, and *Mecp2*^{het}) were prepared by injecting a Cre-dependent AAV-expressing *GCaMP7s* and optical fiber implants in the auditory cortex as described above. Bulk *GCaMP*-detected calcium signals from PVins were measured using a custom setup as described previously (Dvorkin and Shea, 2022). Subjects were head fixed by bolting the titanium bar implant to a frame suspended above a freely

rotating foam wheel for the duration of the recording. An optical cable (200 μm , 0.39 NA) coupled to the fiber implant was used to deliver 473 nm and 565 nm light from a pair of LEDs (LEDD1B, Thorlabs). Green emitted light was used to measure the activity-dependent fluorescence of GCaMP, whereas red emitted light was used to monitor and correct for potential movement or optical coupling artifacts unrelated to neural activity. No such artifacts were ever detected in our head-fixed recordings. Light from each LED was modulated at 211 Hz but 180° out of phase. Before each recording session, the power of the light emitted at the tip of the patch cable was measured with a power meter (PM100D, Thorlabs) and manually adjusted to 30–33 μW .

Emitted light was split into separate green and red paths, bandpass filtered (Chroma Technologies), and detected by separate photodiodes (Newport). Photodiode signals were digitally sampled at 6100 Hz via a data acquisition board (NI USB-6211, National Instruments). As head-fixed recordings were uncontaminated by movement artifacts, only the green emission signal was used to compute $\Delta F/F$ by performing the following steps. For each day of recording, first we measured the peak of each cycle, effectively generating a waveform at 211 Hz sampling rate. We low-pass filtered the data at 15 Hz. Then to account for photobleaching, we fit the trace with a second-order exponential function, which we subtracted from the signal. Finally, we subtracted the mean of the whole trace and divided the result by the same mean. To facilitate direct comparisons between different animals, all fluorescence traces from a given animal were converted to a Z-score using the mean and SD of the entire dataset for that animal.

The same USV stimulus set was presented during fiber photometric recordings as described for electrophysiology recordings with an interstimulus interval of 10 s. Custom MATLAB software was used to present stimuli and acquire data via hardware from National Instruments.

Experimental design and statistical analysis

All data visualization and statistical analysis was performed in MATLAB or Prism (GraphPad) software. Unless otherwise noted, values are reported as mean \pm SEM. Behavioral latency data were analyzed with a two-way ANOVA (with factors of time and genotype/treatment) and where warranted, *post hoc* comparisons were made. All histology was performed in batches wherein one subject from each experimental group was represented, and the scorer was blinded to the group. Per-cell PV intensity was Z-scored within each batch, and for PNN counts, in each batch a threshold was applied at the mean +2 SD for all sections in a batch. Only PNNs visible after thresholding were counted. Significant differences in PV intensity and PNN counts were statistically analyzed with a one-way ANOVA.

Spike2 software (Cambridge Electronic Design) was used to manually threshold and sort single-unit spike shapes based on principal components analysis (PCA) clustering. A total of 287 individual neurons were included in the analysis. Several previous studies, including work from our lab, have identified distinct properties of PVin waveforms, including a narrow spike shape, nearly symmetrical positive and negative peak amplitudes, and elevated firing rates (Cohen and Mizrahi, 2015; Lau et al., 2020). We combined our current dataset with another 26 neuronal recordings previously collected in our lab that used photoidentification of PVins expressing the optogenetic activator ChR2. Each of the total 313 neurons was represented by a vector of 28 points defining the mean spike shape plus the ongoing firing rate of the cell. The 313×29 matrix was used as the input to a PCA analysis, and the result was analyzed by *k*-means clustering ($k = 3$). All optically identified neurons were contained within a single cluster; therefore, the neurons in that cluster were designated as putatively PVins.

Peristimulus time histograms (PSTHs; 10 ms bin size) were constructed of the mean firing rate of each cell in response to each stimulus (i.e., cell-stimulus pairs), and bin values were transformed to Z-scores for each cell. Significant responses were identified among all cell-stimulus pairs with a bootstrap procedure as follows. If a given stimulus was presented n times, n windows of 150 ms each were randomly chosen from the entire duration of spiking recorded for that neuron, and the mean spike rate for all n windows was calculated. This was repeated 10,000 times to generate a null distribution of randomized spiking rates.

Significant cell-stimulus pairs were identified as those for which the actual mean response in the 150 ms after the stimulus onset fell within the upper or lower 2.5% of the spiking rate null distribution. Cells that lacked a significant response to any stimulus were discarded from the analysis. The response for each cell-stimulus pair was computed as the integrated area under the first 200 ms of the PSTH in units of Z-score \cdot s. Mean responses across experimental groups were statistically compared with Mann–Whitney *U* tests.

For fiber photometry data, to compare fluorescence signals across animals and over time, $\Delta F/F$ signals collected from each animal were transformed to a Z-score. Responses to each stimulus were computed as the integrated area under the mean response curve in units of Z-score \cdot s. For each genotype, mean responses to auditory stimuli at the pup-naive time point were compared with mean responses measured at a postnaive time point (P3–P5) with a paired *t* test.

Results

Acquisition of pup retrieval is delayed by loss of *Mecp2* in parvalbumin interneurons

We previously showed that female *Mecp2*^{het} mice fail to reliably retrieve pups, even after 5 d of cohabitation with a WT dam and her litter (Krishnan et al., 2017). We also found that when mice were crossed between PV-Cre and *Mecp2*^{lox}, PV-*Mecp2* mutants were initially slower to retrieve compared with PV-*Mecp2* WT subjects (Krishnan et al., 2017). This raised the possibility that certain cell types within the auditory cortex might be more important than others for the neural plasticity that facilitates retrieval. Here, we replicate that finding, and we compare the results with our observations from knocking out *Mecp2* in several other genetically restricted neuronal populations.

We used several mouse lines expressing Cre-recombinase in specific cell types in conjunction with *Mecp2*^{lox} mice to restrict *Mecp2* knockout to three distinct populations of GABAergic inhibitory neurons, namely, parvalbumin-expressing PVins, somatostatin (SST)-expressing SSTins, and vasoactive intestinal peptide (VIP)-expressing VIPins. We also used the Emx1-Cre line to restrict *Mecp2* knockout to the majority (~90%) of excitatory cortical pyramidal neurons (Briata et al., 1996) (Fig. 1A). Female subjects were cohoused with a pregnant WT CBA female, and beginning on P0, were tested daily in a pup retrieval assay (Fig. 1B; see above, Materials and Methods; Krishnan et al., 2017). Cohousing gives the virgin females the opportunity to observe and participate in interactions with pups (Carcea et al., 2021). Therefore, their improvement in performance over time reflects only the influence of experience, not hormonal changes related to pregnancy and parturition.

PV-*Mecp2* mutants showed significantly longer retrieval latency scores compared with PV-*Mecp2* WT on P0. However, these subjects improved over time, matching the performance of PV-*Mecp2* WT mice by P1 (Fig. 1C). A two-way mixed effects ANOVA revealed significant effects of time (day; $F = 9.21$, $p < 0.001$) and genotype ($F = 9.41$, $p < 0.01$), but not an interaction between those variables ($F = 1.94$, $p = 0.15$). *Post hoc* testing revealed a significant difference between the mutant and WT groups for P0 only (Sidak's test, $p < 0.001$). Individual unpaired comparisons for each day detected a significant difference between genotypes only on P0 ($n = 25$ mutant, 15 WT; Mann–Whitney corrected for multiple comparisons, $p < 0.01$). Therefore, PV-*Mecp2* mutants showed a transient disruption in pup retrieval.

To assess the specificity of this result to the PVin population, as opposed to other interneuron types, we ran the same experiment with mice in which *Mecp2* was knocked out in one of two

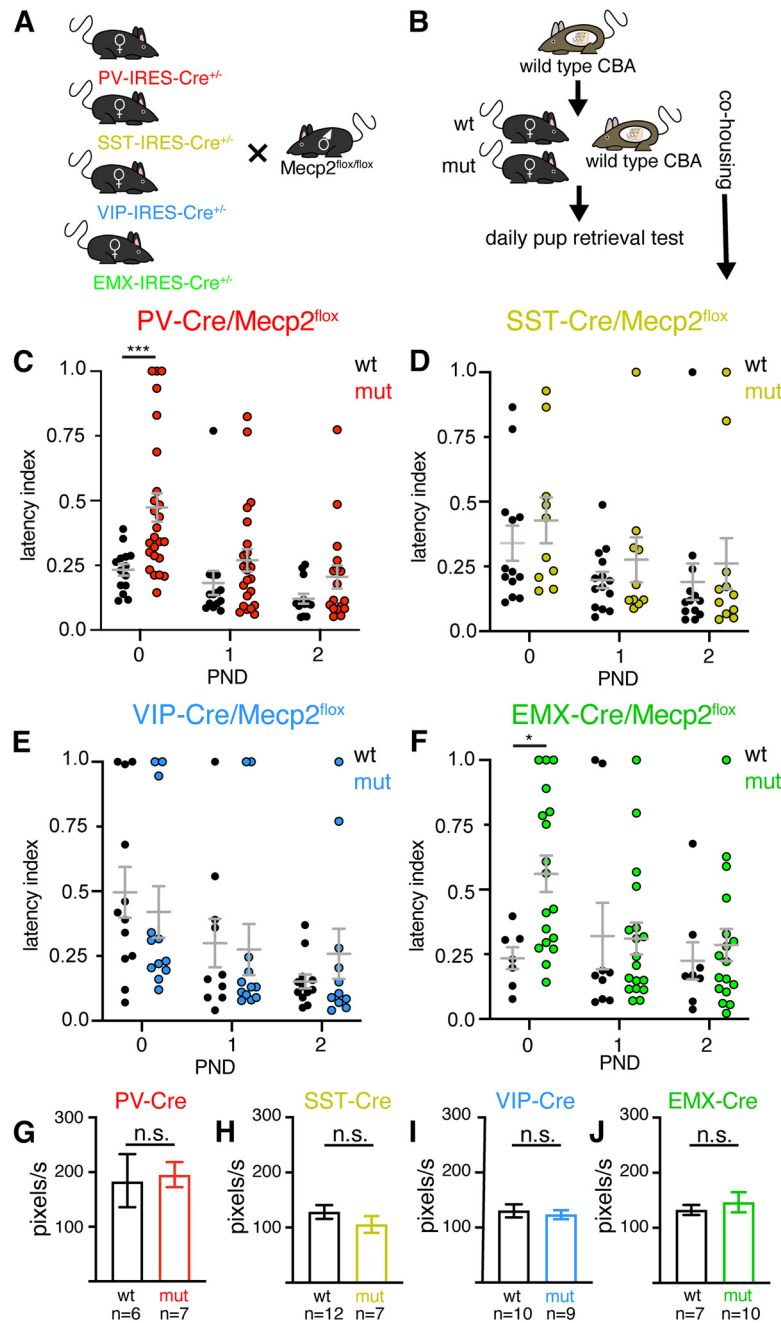


Figure 1. Cell-type-specific deletion of *Mecp2* has varying effects on pup retrieval behavior. **A**, Schematic of mouse lines crossed to achieve selective *Mecp2* deletion in different neuron types. **B**, Schematic of cohousing and retrieval behavior protocol. **C–F**, Scatterplots of retrieval latency comparing performance of cell-type-specific *Mecp2* mutants to that of their littermate controls for PV-Cre (**C**), SST-Cre (**D**), VIP-Cre (**E**), and Emx1-Cre (**F**) lines crossed with *Mecp2*^{flox} mice. Emergence of pup retrieval was delayed in PV-*Mecp2* mutants relative to controls (**C**). A two-way ANOVA revealed significant main effects for time (day of testing; $F = 9.21$, $p < 0.001$) and genotype ($F = 9.41$, $p < 0.01$) but not an interaction ($F = 1.94$, $p = 0.15$). *Post hoc* tests revealed a significant difference between mutant and WT animals on P0 only ($n = 14$ controls, latency, 0.17 ± 0.03 ; $n = 25$ mutants, latency, 0.32 ± 0.08 ; Sidak's test, $***p < 0.001$). Timing of emergence of pup retrieval did not differ between SST-*Mecp2* mutants and controls (**D**). A two-way ANOVA revealed a significant main effect for time (day of testing; $F = 8.98$, $p < 0.01$), but not for genotype or for an interaction. *Post hoc* tests revealed no significant difference between mutant and WT animals on any day (Sidak's test, $p > 0.05$). Emergence of pup retrieval did not differ between VIP-*Mecp2* mutants and controls (**E**). A two-way ANOVA revealed a significant main effect for time/day (VIP-*Mecp2*, $F = 7.50$, $p < 0.01$), but not for genotype, nor an interaction between those variables. *Post hoc* tests revealed no significant difference between mutant and WT animals on any day of testing (Sidak's test, $p > 0.05$). Emergence of pup retrieval was delayed in Emx1-*Mecp2* mutants relative to controls (**F**). A two-way ANOVA revealed a significant effect only for the interaction between time and genotype ($F = 3.86$, $p < 0.05$), but neither a main effect for genotype ($F = 2.45$, $p = 0.13$) nor day ($F = 2.13$, $p = 0.14$). A *post hoc* test revealed a significant difference between mutant and WT animals for P0 only ($n = 7$ controls, latency, 0.26 ± 0.03 ; $n = 18$ mutants, latency, 0.39 ± 0.09 ; Sidak's test, $*p < 0.05$). **G–J**, Bar plots of mean velocity of mice during retrieval sessions on P0, comparing mutants (*Mecp2*^{flox}) with controls for PV-Cre (**G**), SST-Cre (**H**), VIP-Cre (**I**), and Emx1-Cre (**J**). No significant difference was found for any of the lines (unpaired *t* test, PV, $p = 0.82$; SST, $p = 0.27$; VIP, $p = 0.63$; EMX, $p = 0.56$).

other major classes of GABAergic inhibitory neurons (SSTins or VIPins; Fig. 1D,E). Two-way mixed effects ANOVAs revealed significant effects for time (day) in both cohorts (SST-*Mecp2*, $F = 8.98$, $p < 0.01$; VIP-*Mecp2*, $F = 7.50$, $p < 0.01$), but not for genotype or for an interaction between those variables. *Post hoc* testing revealed no difference between mutant and WT groups for any day of testing (Sidak's test, $p > 0.05$). Individual unpaired comparisons for each day also failed to detect significant differences between genotypes on any day ($p > 0.05$) for either line. Therefore, neither SST-*Mecp2* mutants nor VIP-*Mecp2* mutants showed a transient disruption in pup retrieval as observed for PV-*Mecp2* subjects.

As a comparison to *Mecp2* deletion in small interneuron populations, we next crossed *Mecp2*^{fllox} mice with the *Emx1-Cre* line to restrict *Mecp2* knockout to ~90% of excitatory neurons in the cortex and hippocampus (Briata et al., 1996). Like PV-*Mecp2* mutants, *Emx1-Mecp2* mutants exhibited a delayed onset of pup retrieval (Fig. 1F). A two-way mixed effects ANOVA revealed a significant effect only for an interaction ($F = 3.86$, $p < 0.05$) but neither a main effect for genotype ($F = 2.45$, $p < 0.13$) nor for day ($F = 2.13$, $p = 0.14$). *Post hoc* testing revealed a significant difference between mutant and WT groups for P0 only (Sidak's test, $p < 0.01$). Individual unpaired comparisons for each day detected a significant difference between genotypes only on P0 ($n = 18$ mutant, 7 WT; Mann-Whitney corrected for multiple comparisons, $p < 0.05$). Therefore, like PV-*Mecp2* mutants, *Emx-Mecp2* mutants showed a transient disruption in pup retrieval. Interestingly, this disruption was comparable in the two groups, despite the disparity in the size of the cell populations. Performance of all mice was unrelated to gross motor deficits, as determined by automated tracking of the animals during retrieval with DeepLabCut software, which showed there was no significant difference in mean velocity between controls and mutants for any of the lines (Fig. 1G–I).

Loss of *Mecp2* only in PVins recapitulates changes of molecular expression seen in *Mecp2*^{het}

High levels of expression of PVin markers (PVs and PNNs) are taken as an indicator of maturity in PVins and are well correlated with reduced capacity for synaptic plasticity and learning in development and adulthood (Pizzorusso et al., 2002; Carulli et al., 2010; de Vivo et al., 2013; Donato et al., 2013; Happel et al., 2014; Hou et al., 2017; Cisneros-Franco and de Villers-Sidani, 2019; reviewed in Rupert and Shea, 2022). Previously, we reported that both markers exhibited overexpression in the auditory cortex of *Mecp2*^{het} after 5 d of exposure of a virgin female to pups (Krishnan et al., 2017). This experience-dependent overexpression was not observed in *Mecp2*^{wt}, and genetic and pharmacological approaches that reversed it restored retrieval performance in *Mecp2*^{het} (Krishnan et al., 2017).

Given that *Mecp2* deletion in PVins, a small population of neurons (~10%), is sufficient to disrupt retrieval behavior (albeit temporarily) and that population is also the locus of key pathologic features in *Mecp2*^{het} models, we hypothesized that the changes to PV and PNN may reflect a cell-autonomous consequence of *Mecp2* deletion from PVins. To test this hypothesis, we compared the level of PV protein and PNN expression by auditory cortex PVins between PV-*Mecp2* mutants and PV-*Mecp2* WT. We did this by performing IHC and confocal microscopy of fixed brain sections from naive mice (no pup exposure), and experienced mice (after pup exposure) at the P1 and P5 time points (Fig. 2Ai–iii, Bi–iii). We quantified per-cell intensity of PV staining and, to minimize batch effects, converted intensities

from each batch to a Z-score. We compared the distribution of Z-scores for each group, focusing on the changes within each genotype across time points as pup experience increased. A one-way ANOVA revealed significant differences among group means ($F = 47.3$, $p < 0.001$). PV-*Mecp2* WT virgin mice showed a drop in PV expression; PV staining intensity was significantly lower on P5 compared with intensities of the naive and P1 cohorts (Fig. 2C, Sidak's test, $p < 0.001$). In contrast, PV-*Mecp2* mutants exhibited an increase in PV expression; PV staining intensity was significantly higher in tissue collected at both P1 and P5 compared with naive animals (Sidak's test, $p < 0.001$).

To quantify changes in PNN expression, we counted high-intensity PNNs in the auditory cortex in the same set of sections analyzed (see above, Materials and Methods). To minimize batch effects, all images were thresholded and binarized at 2 SDs above the mean pixel value for each staining batch, and the counts of PNNs per section were Z-scored within each batch. An analysis of all groups detected significant differences among the groups (one-way ANOVA; $F = 4.30$, $p < 0.01$; Fig. 2D). *Post hoc* tests comparing PNN counts from experienced mice at P1 and P5 to counts at the naive time point for both genotypes showed PNN counts per section were only significantly higher on P1 in PV-*Mecp2* mutants (Sidak's test, $p < 0.05$). In light of all these observations, we conclude that deletion of *Mecp2* in PVins is sufficient to at least transiently evoke overexpression of molecular markers closely associated with suppression of plasticity on exposure to pups.

PV-*Mecp2* mutants lack the auditory cortical disinhibition triggered by pup exposure in WT

Our next goal was to determine whether deletion of *Mecp2* only in PVins was sufficient to reproduce the neurophysiological changes we observed in the auditory cortex of pup-experienced *Mecp2*^{het} mice. We found that pup-experienced *Mecp2*^{wt} mice exhibited a dramatic decrease in spiking output by auditory cortex PVins relative to that from naive females (Lau et al., 2020). Moreover, we discovered that this disinhibition of the auditory cortex by PVins was absent in *Mecp2*^{het} (Lau et al., 2020). We hypothesized that deletion of *Mecp2* only from PVins may affect their stimulus-evoked firing in a cell-autonomous manner. To test this hypothesis, we made loose-patch, single-unit electrophysiological recordings from auditory cortical neurons in awake head-fixed animals of both genotypes at naive and after pup-experienced time points. We made neuronal recordings from four experimental groups of mice—PV-*Mecp2* mutant mice that were naive to pups (PV-Cre/*Mecp2* mutant Naive; $n = 7$ mice), PV-*Mecp2* mutant mice that cohabitated with a WT dam and her pups for >5 d (PV-Cre/*Mecp2* mutant experienced; $n = 10$ mice), PV-Cre/*Mecp2* WT control littermates without pup experience (PV-Cre/*Mecp2* WT Naive; $n = 15$ mice), and WT littermates that experienced cohabitation (PV-Cre/*Mecp2* WT experienced; $n = 21$ mice).

As previously reported (Wu et al., 2008; Oswald and Reyes, 2011; Cohen and Mizrahi, 2015; Lau et al., 2020), PVins and non-PV neurons had characteristic spike shapes that could be distinguished by their features. We therefore combined the neurons we recorded here with a wild-type dataset from a previous study (Lau et al., 2020) in which we optically identified ChR2-expressing PVins. We identified putative clusters of PVins and non-PV neurons in a PCA with a *k*-means clustering algorithm (see above, Materials and Methods). Average spike waveforms for our putatively identified populations of cells are

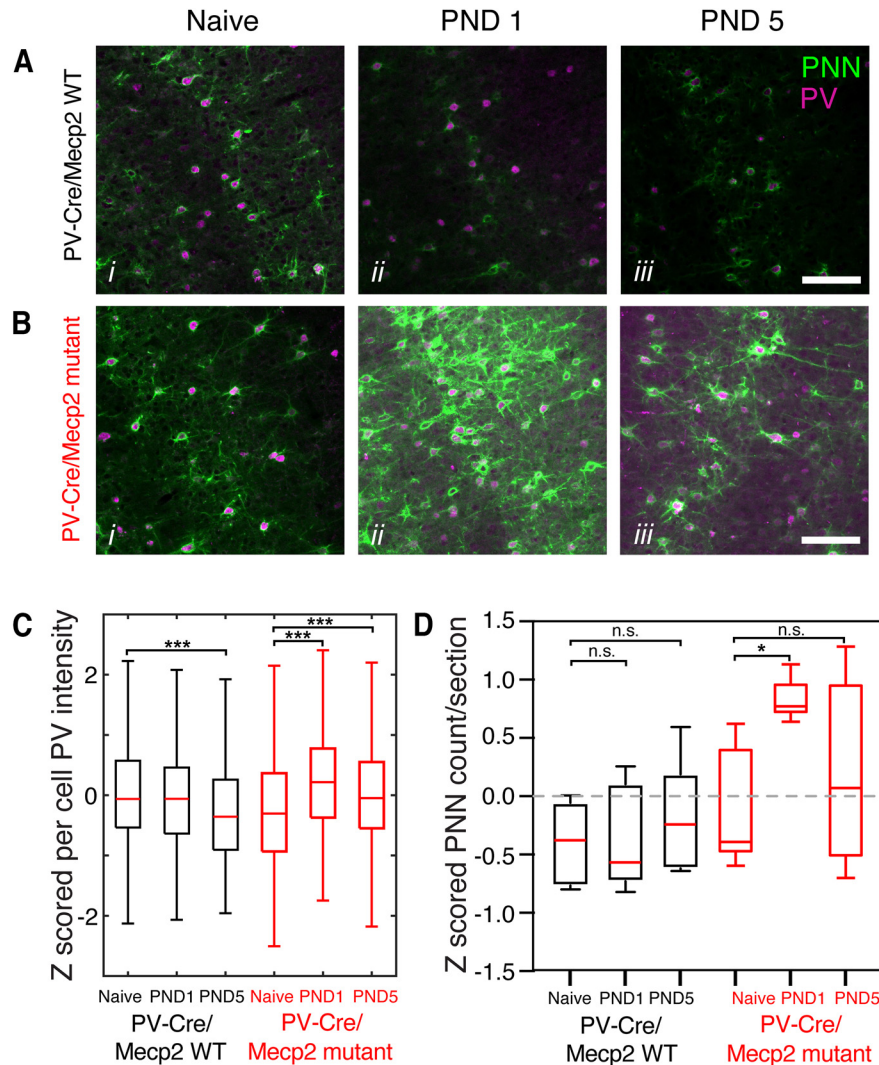


Figure 2. Selective deletion of *Mecp2* in PVins recapitulates changes of molecular expression seen in *Mecp2*^{het}. **Ai–iii**, Series of photomicrographs of example sections of the auditory cortex taken from a PV-*Mecp2* WT naive mouse (*i*), a mouse after 2 d of cohabitation (P1; *ii*), and a mouse after 6 d of cohabitation (P5; *iii*). All sections were stained with IHC using an antibody for parvalbumin (purple) and a biotinylated lectin from *Wisteria floribunda* for PNNs (green). Scale bar, 200 μ m. **Bi–iii**, Same as **Ai–iii** but for sections taken from PV-*Mecp2* mutants. **C**, Box plot of the distributions of per-cell intensity of parvalbumin staining. All histology was run in six batches, with one brain from each genotype condition group represented in each batch. All individual neuron intensities were Z-scored per batch. From left to right, The total number of neurons in each group is 1006, 996, 757, 1108, 1084, 1063. A one-way ANOVA detected differences among the groups ($F = 47.3$, $p < 0.001$). *Post hoc* testing revealed a significant decrease of mean PV intensity in PV-*Mecp2* WT on P5 compared with naive mice (naive latency, 0.076 ± 0.03 Z-score; P5 latency, 0.25 ± 0.03 Z-score; Tukey's test, $***p < 0.001$). In contrast, PV-*Mecp2* mutant mice had higher mean per cell intensity PV staining on P1 (0.31 ± 0.03 Z-score) and P5 (0.047 ± 0.03 Z-score) compared with naive mice (-0.25 ± 0.03 Z-score; Tukey's test, $***p < 0.001$). **D**, Box plot of mean high intensity PNNs per section, comparing all six groups of mice. One mouse from each group was processed in each batch with total of five batches. Per-section counts were Z-scored for all sections in each batch. Considering all groups, there was a significant difference among them (one-way ANOVA, $F = 4.3$, $p < 0.01$). *Post hoc* comparisons of each experienced time point to the naive time point for each genotype showed that PV-*Mecp2* mutant mice on P1 had significantly more high-intensity PNNs per section than naive PV-*Mecp2* mutant mice ($n = 5$ mice/group; naive mutant, -0.11 ± 0.23 Z-score; mutant P1, 0.83 ± 0.08 Z-score; Sidak's test, $*p < 0.05$).

plotted as corresponding color traces in Figure 3, B and C. PVins had particularly narrow spike waveforms and were more symmetrical in amplitude around the baseline; non-PV neurons were wider and had more prominent positive peaks (Fig. 3B,C). Despite our use of a novel PCA-based sorting method, our results were very consistent with previous classification results from our group and others (Wu et al., 2008; Oswald and Reyes, 2011; Cohen and Mizrahi, 2015; Lau et al., 2020).

We first examined the responses of non-PV neurons from each group to a library of eight USVs recorded from pups that were 2–4 d old (Lau et al., 2020). We observed that individual non-PV neurons often exhibited distinct responses to different USVs, responding with either increases or decreases in firing. Therefore, we identified all cell-call pairs (mean responses of one

neuron to one stimulus) that exhibited a statistically significant change in firing rate as assessed with a bootstrap procedure (see above, Materials and Methods). A PSTH (bin size, 10 ms) was constructed to visualize the mean response of each cell to each stimulus, and the bins of all PSTHs from each cell were transformed to a Z-score.

Heat maps in Figure 4, A and B, depict 2D PSTHs that each represent the mean responses for all cell-call pairs from one of the four groups of wild types (Fig. 4A) and mutants (Fig. 4B). Rows in each 2D PSTH are sorted from the largest firing decrease to the largest firing increase measured in the 200 ms window after stimulus onset. We separately compared the mean of all excitatory responses (stimulus-driven increase in firing rate) and the mean of all inhibitory responses (stimulus-driven

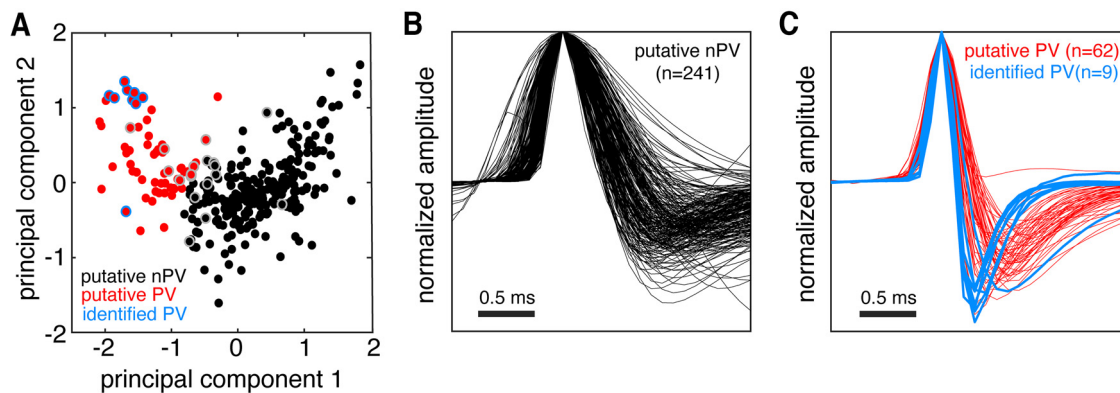


Figure 3. Classification of PVin and non-PV single-unit recordings by spike waveform and firing rate. **A**, Scatterplot showing the results of a principal components analysis and *k*-means clustering analysis of 313 auditory cortex neurons based on the mean spike waveform and baseline firing rate. Red points denote putative PVs, black points denote putative non-PV neurons, points outlined in blue denote a subset of optically tagged PVs, and points outlined in gray denote inconclusive optical identification results. **B**, Plot of all mean waveforms from putative non-PV neurons ($n = 241$). **C**, Plot of all mean waveforms from putatively identified PVs ($n = 71$).

decrease in firing rate) between naive and pup-experienced groups for each genotype. Figure 4, *C* and *D*, depict mean \pm SEM traces for each sign of response. Gray traces represent recordings collected from naive mice, and purple traces represent recordings collected from pup-experienced mice. We integrated the area under the curve (AUC) for each cell-call pair and compared the distribution of response magnitudes between naive and experienced mice cohorts. Figure 4*E* summarizes the results of these comparisons for PV-*Mecp2* and WT mice. In WT mice, mean inhibitory responses were significantly weaker in mice that had cohousing experience with pups relative to mice that lacked pup exposure ($n = 54$ naive and 44 experienced cell-call pairs; Mann-Whitney *U* test, $p < 0.01$). Mean excitatory responses were unchanged between naive and experienced mice ($n = 108$ naive and 72 experienced cell-call pairs; Mann-Whitney *U* test, $p = 0.09$). Figure 4*F* shows the corresponding results for PV-*Mecp2* mutant mice. In these mice, mean inhibitory responses were significantly stronger in pup-experienced mice than they were in pup-naive mice ($n = 31$ naive and 30 experienced cell-call pairs; Mann-Whitney *U* test, $p < 0.001$). As in WT mice, mean excitatory responses were unchanged between naive and experienced PV-*Mecp2* mutant mice ($n = 60$ naive and 45 experienced cell-call pairs; Mann-Whitney *U* test, $p = 0.61$).

We performed a similar analysis on recordings collected from putative PVins (Fig. 5). In this case, because all USV responses we observed in PVins evoked increased spiking, we included all responses to stimuli for all neurons that had a significant response to at least one USV. As in Figure 4, a PSTH for each cell-call pair was constructed and organized into a 2D PSTH for each group where rows were sorted from the weakest response to the strongest response (Fig. 5*A,B*). Traces of mean \pm SEM firing rate across all PVins cell-call pairs are plotted for naive mice (gray) and experienced mice (purple) of each genotype (Fig. 5*C,D*). Consistent with our previous report (Lau et al., 2020), auditory cortex PVins in experienced WT mice exhibited dramatically and significantly weaker responses to USVs compared with PVins in naive WT mice (Fig. 5*B*; $n = 80$ naive and 104 experienced cell-call pairs; Mann-Whitney *U* test, $p < 0.001$). In contrast, mean responses of PVins were unchanged between naive and pup-experienced PV-*Mecp2* mutants ($n = 64$ naive and 32 experienced cell-call pairs; Mann-Whitney *U* test, $p = 0.61$). Based on all the data from our electrophysiology experiments, we conclude that selective deletion of *Mecp2* in PVins is

sufficient for disrupting the auditory cortical disinhibition that is triggered by exposure to pups as observed in WT virgin mice.

Optical recordings reveal that PVin disinhibition depends on experience and *Mecp2* in PVins

One important limitation of our electrophysiology data is that it was not practical to conduct recordings from the same subjects in both naive and pup-experienced states. A more powerful experimental design would be to measure PVin activity in the same animal over the duration of its cohabitation experience with pups. A second limitation is that these recordings yield information about only one PVin at a time. It would be useful to complement those data with recordings of the neuronal population. Therefore, we used fiber photometry to make longitudinal measurements of widespread PVin activity in response to auditory stimuli as mice advanced from the pup-naive state through several days of cohabitation. Subjects were prepared by making injections of Cre-dependent AAV-DIO-GCaMP7s into the auditory cortex and by implanting an optical fiber at the same location (see above, Materials and Methods). Because PV-Cre was necessary in all mice to express GCaMP, subjects were either *Mecp2*^{fllox+/fllox+} (PV-*Mecp2* mutant) or *Mecp2*^{fllox-/fllox-} (PV-*Mecp2* WT). We also included a group of mice that were PV-Cre⁺ and *Mecp2*^{het} to compare results between PVin-selective *Mecp2* deletion to the nonconditional, mosaic model. We conducted daily recording sessions from head-fixed mice, presenting the same set of USVs used in the neuronal recordings.

Figure 6*A* shows example data for three different mice. The top row of plots represents data from a PV-*Mecp2* WT subject. Each row in the heat maps is a single-trial response to one specific USV. Trials above the green horizontal line were taken from sessions before cohabitation (naive state), and trials below the line were taken from sessions on P3–P5. Each call, denoted by the black vertical tick mark, elicited an abrupt increase in fluorescence that decayed over the course of 2 s. Below each heat map is a trace of the mean \pm SEM calcium response from all naive trials (gray) and trials collected on days 3–5 of pup experience (purple).

We quantified the responses to calls as the mean AUC across trials and stimuli and compared that measure for all mice before and after pup exposure (Fig. 6*B*). In agreement with our single-neuron data, we found that the auditory cortex PVin population in PV-*Mecp2* WT subjects exhibited consistently weaker mean responses to USVs after several days of pup exposure compared

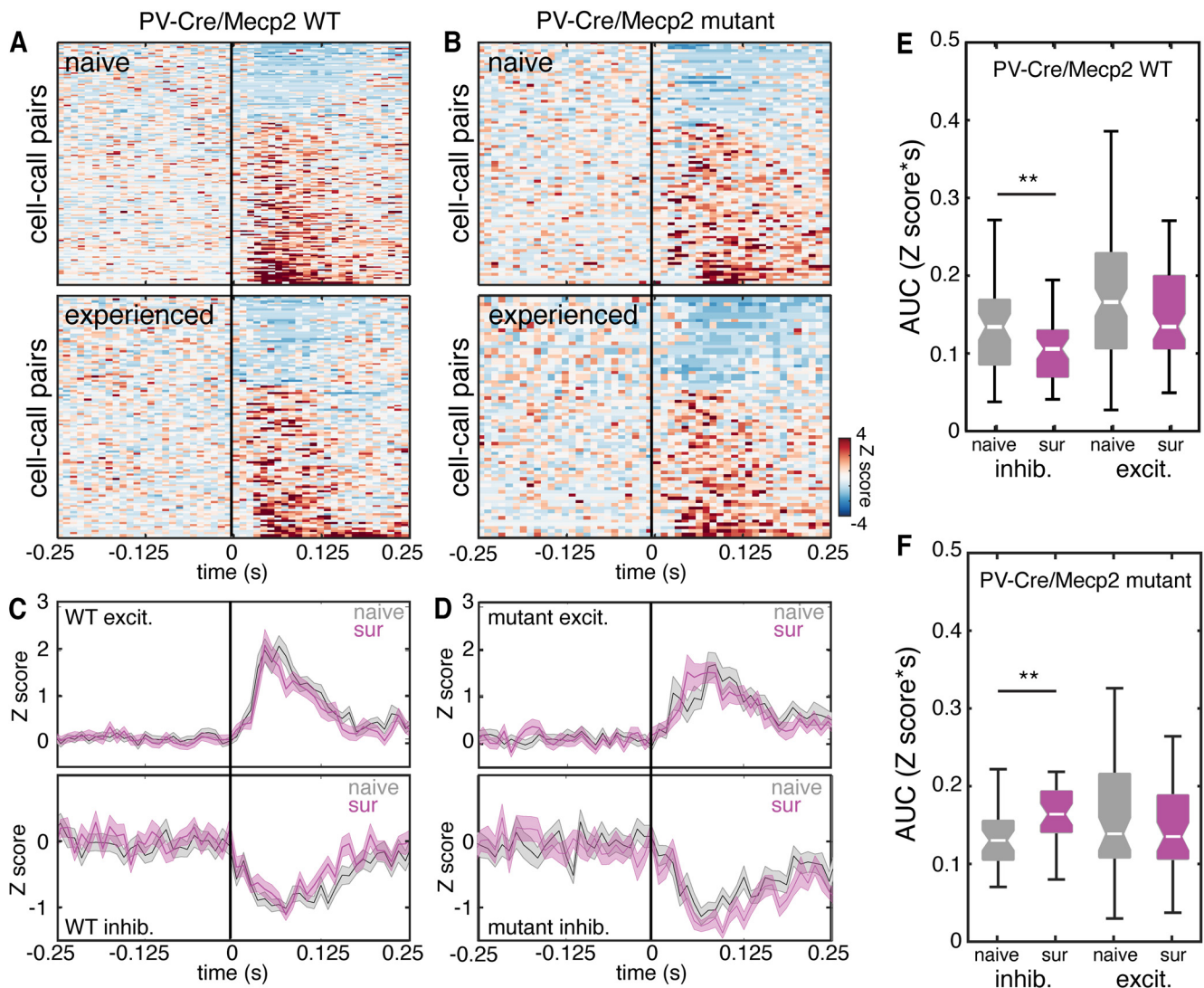


Figure 4. Selective deletion of *Mecp2* in PVins recapitulates the suppression of non-PV neuron inhibitory plasticity seen in *Mecp2*^{het}. **A**, Two-dimensional PSTHs representing the mean responses for all non-PV cell-call pairs with significant responses to USVs from naive (top) and experienced (bottom) PV-*Mecp2* WT mice. Each row within the PSTHs represents the Z-scored response of one cell-call pair. Rows are sorted from the greatest stimulus-evoked decrease in firing rate to the greatest stimulus-evoked increase in firing rate. Response window of 200 ms after the stimulus onset is marked by the vertical black line. **B**, Same as **A**, but data are taken from auditory cortex recordings in PV-*Mecp2* mutant mice. **C**, Mean \pm SEM traces for excitatory responses (top) and inhibitory responses (bottom), comparing data from naive (gray) and experienced (purple) PV-*Mecp2* WT mice. **D**, Same as **C**, but the data are from PV-*Mecp2* mutant mice. **E**, Box plot of the integrated AUC for each non-PV cell-call pair recorded from PV-*Mecp2* WT mice comparing the distribution of inhibitory and excitatory response magnitudes between naive mice and experienced mice. Mean inhibitory responses were significantly weaker in pup-experienced mice relative to pup-naive mice (naive, $n = 54$ cell-call pairs, 0.132 ± 0.01 Z-score*s; experienced, $n = 44$ cell-call pairs, 0.101 ± 0.01 Z-score*s; Mann-Whitney *U* test, ** $p < 0.01$). Mean excitatory responses were unchanged between naive and experienced mice (naive, $n = 108$ cell-call pairs, 0.195 ± 0.01 Z-score*s; experienced, $n = 72$ cell-call pairs, 0.161 ± 0.01 Z-score*s; Mann-Whitney *U* test, $p = 0.09$). **F**, Same as **E**, but data are from non-PV cell-call pairs recorded from PV-*Mecp2* mutant mice. Mean auditory cortex inhibitory responses were significantly stronger in experienced mice than they were in pup-naive mice (naive, $n = 31$ cell-call pairs, 0.134 ± 0.01 ; experienced, $n = 30$ cell-call pairs, 0.170 ± 0.01 ; Mann-Whitney *U* test, *** $p < 0.001$). As in WT mice, mean excitatory responses were unchanged between naive and experienced PV-*Mecp2* mutants (naive, $n = 60$ cell-call pairs 0.171 ± 0.01 , Z-score*s; experienced, $n = 45$ cell-call pairs, 0.160 ± 0.01 Z-score*s; Mann-Whitney *U* test, $p = 0.61$).

with responses measured in the naive state (Fig. 6B; $n = 8$ mice; paired *t* test with Bonferroni correction, $p < 0.001$). Importantly, this drop in PVin responses required experience; pup-naive control mice that were recorded on the same schedule did not show a significant decrease in PVin activity in response to the same stimulus set presented to the experienced mice (Fig. 6B; $n = 6$ mice; paired *t* test, $p = 0.40$). Neither *Mecp2*^{het} ($n = 8$ mice; paired *t* test, $p = 0.16$) nor PV-*Mecp2* mutants ($n = 5$ mice; paired *t* test, $p = 0.56$) showed a significant decrease in the responses of PVins to USVs. We also presented these same mice with a library of pure tones, and we obtained the same result. Stimulus-driven activity of the PVins in auditory cortex was

significantly decreased in response to tones (Fig. 6C; $n = 8$ mice; paired *t* test with Bonferroni correction, $p < 0.01$). This was not true of unexposed control mice (Fig. 6C; $n = 6$ mice; paired *t* test, $p = 0.51$), *Mecp2*^{het} ($n = 8$ mice; paired *t* test, $p = 0.48$), or PV-*Mecp2* mutants ($n = 5$ mice; paired *t* test, $p = 0.72$).

Acquisition of pup retrieval is delayed by adult loss of *Mecp2* in auditory cortical PVins

All the above observations indicate that PVins play an important early role in initiating cortical plasticity in response to sensory and social experience with pups. Loss of *Mecp2* exclusively in

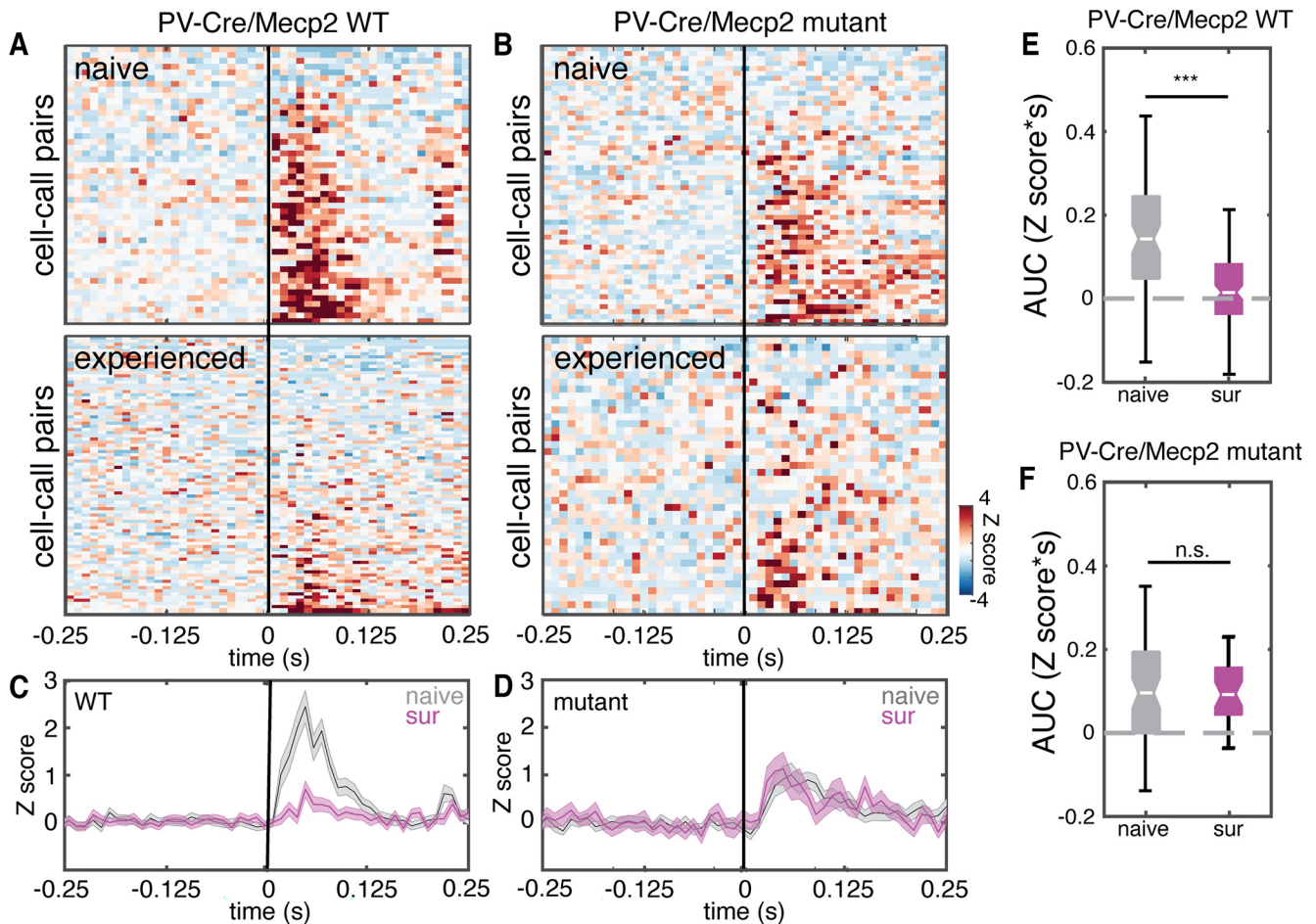


Figure 5. Selective deletion of *Mecp2* in PVins recapitulates the suppression of PVin neuron inhibitory plasticity seen in *Mecp2*^{het}. **A**, Two-dimensional-PSTHs representing the mean responses for all PVin cell-call pairs with significant responses to any USV from naive (top) and experienced (bottom) PV-Mecp2 WT mice. Each row within the PSTHs represents the Z-scored response of one cell-call pair. Rows are sorted from the greatest stimulus-evoked decrease in firing rate to the greatest stimulus-evoked increase in firing rate. Response window of 200 ms after the stimulus onset is marked by the vertical black line. **B**, Same as **A**, but the data are from PV-Mecp2 mutant mice. **C**, Mean \pm SEM traces for USV responses of all cell-call pairs, comparing data from pup-naive (gray) and pup-experienced (purple) WT mice. **D**, Same as **C**, but the data are from PV-Mecp2 mutant mice. **E**, Box plot of the integrated AUC for each PVin cell-call pair in PV-Mecp2 WT mice comparing response magnitudes between naive mice and experienced mice. Mean responses were significantly weaker in mice that had experience with pups relative to pup-naive mice (naive, $n = 80$ cell-call pairs, 0.147 ± 0.03 Z-score*s; experienced, $n = 104$ cell-call pairs, 0.035 ± 0.01 Z-score*s; Mann–Whitney *U* test, *** $p = 0.001$). **F**, Same as **E**, but data are from PVin cell-call pairs collected from PV-Mecp2 mutant mice. In contrast to WT mice, PVin responses were unchanged between naive and experienced PV-Mecp2 mutant mice (naive, $n = 64$ cell-call pairs 0.087 ± 0.01 Z-score*s; experienced, $n = 32$ cell-call pairs, 0.095 ± 0.01 Z-score*s; Mann–Whitney *U* test, $p = 0.79$).

this neuronal subtype, which represents only $\sim 10\%$ of the neurons in the neocortex, replicates many key features of the maternal behavioral and neural pathology seen in *Mecp2*^{het}. However, our approach of crossing PV-Cre mice with *Mecp2*^{lox} does not specifically implicate PVins in the auditory cortex, nor does it distinguish between an acute requirement for *Mecp2* in PVins in adulthood (e.g., during the initial exposure of the virgin mouse to pups) and an earlier requirement for *Mecp2* in PVins for proper development of the auditory cortex to support later plasticity. We therefore devised an intersectional viral-genetic strategy to address this limitation.

Figure 7A is a schematic depiction of our strategy to target *Mecp2* only in PVins in the auditory cortex and only after cortical development (see above, Materials and Methods). Briefly, we crossed *Mecp2*^{lox} mice with a line that expresses Flp recombinase in PV neurons, and then at 6 weeks of age, bilaterally injected the auditory cortex with either an AAV driving the Flp-dependent expression of Cre recombinase and an HA tag (Flp-Flox) or a control vector expressing GFP (GFP-Flox).

We compared the pup retrieval performance on P0 Flp-Flox subjects to that of GFP-Flox mice and found that mean retrieval

latency was longer for Flp-Flox subjects (Fig. 7B). A one-way ANOVA was used to compare P0 retrieval latencies between those groups and also between PV-Mecp2 mutant and PV-Mecp2 WT. Significant differences were detected among the groups ($F = 5.02$, $p < 0.01$), and *post hoc* testing detected significantly longer latencies for the Flp-Flox group ($n = 12$ Flp-Flox mice, $n = 12$ GFP-Flox mice; Sidak's test, $p < 0.05$) and the PV-Mecp2 mutant group ($n = 25$ PV-Mecp2 mutant mice, $n = 14$ PV-Mecp2 WT mice; Sidak's test, $p < 0.001$) when compared with their respective controls.

Discussion

Several lines of evidence from our previous work on *Mecp2*^{het} mice strongly suggested that dysregulation of PVins in auditory cortex is a critical feature of the neuropathology underlying their failure to learn to perform pup retrieval behavior. Specifically, in the auditory cortices of *Mecp2*^{het} virgin females cohoused with a dam and her litter, we observed dramatic overexpression of markers associated with PVins (parvalbumin protein and perineuronal nets) that are known to be antagonistic to plasticity

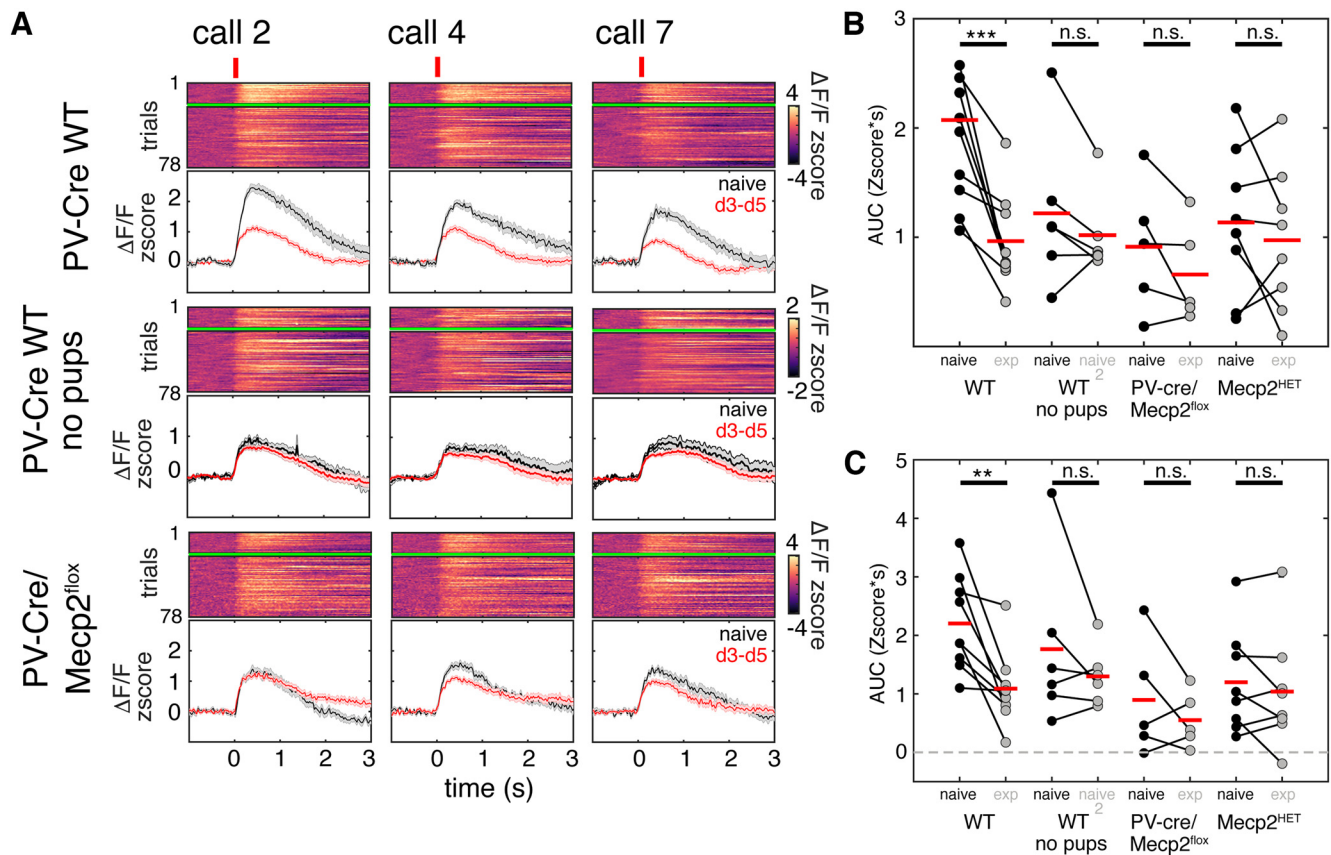


Figure 6. PVin disinhibition is widespread and depends on experience and presence of *Mecp2* in PVin. **A**, Comparison of longitudinal fiber photometry data from three sample subjects. Fluctuations in bulk fluorescence were measured using GCaMP7s expressed in auditory cortical PVins. Each column shows the responses of each mouse to a different USV call exemplar. Top, Data from a PV-*Mecp2* WT mouse. Middle, Data from a PV-*Mecp2* WT mouse that was never introduced to or cohoused with pups. Bottom, Data from a PV-*Mecp2* mutant mouse. The heat maps depict the response to each USV over many trials gathered over several days. Each heat map row is one trial; those above the green line were taken from sessions before pup exposure (naive time point), and those below the line were taken from sessions on P3–P5. Below each heat map is a plot of mean \pm SEM fluorescence traces from naive (gray) and experienced (purple) time points. The onset of call playback is marked with a black tick above the heat map. **B**, Scatterplot of mean naive and experienced PVin responses to all USVs for all mice in each experimental condition. Responses were quantified as the AUC of the Z-scored fluorescence trace during the first 2 s after stimulus onset. WT mice showed a consistent and significant decrease in response strength to USVs between naive trials and during trials on days 3–5 of pup experience ($n = 8$ mice; naive, 2.46 ± 0.79 Z-score*s; experienced, 1.03 ± 0.57 Z-score*s; paired t test, $p^{***} < 0.001$). No significant differences between the early time point and the late time point responses were found for WT mice that were not exposed to pups but were imaged during USV playback on the same schedule ($n = 6$ mice; naive, 1.57 ± 1.0 Z-score*s; experienced, 1.24 ± 0.61 Z-score*s; paired t test, $p = 0.14$), PV-*Mecp2* mutant mice ($n = 5$ mice; naive, 1.61 ± 1.2 Z-score*s; experienced, 1.29 ± 0.68 Z-score*s; paired t test, $p = 0.23$), or *Mecp2*^{HET} ($n = 8$; naive, 1.24 ± 0.77 Z-score*s; experienced, 1.11 ± 0.83 Z-score*s; paired t test, $p = 0.62$). **C**, Identical data from the same mice, but pure tones were presented instead of calls. Responses to tones in WT mice were significantly decreased during trials on days 3–5 of pup experience compared with naive trials ($n = 8$ mice; naive, 2.17 ± 0.29 Z-score*s; experienced, 0.92 ± 0.13 Z-score*s; paired t test, $p^{**} < 0.01$). No significant differences were found for pup-naive WT mice ($n = 6$ mice; naive, 1.53 ± 0.60 Z-score*s; experienced, 1.09 ± 0.18 Z-score*s; paired t test, $p = 0.51$), PV-*Mecp2* mutant mice ($n = 5$ mice; naive, 0.89 ± 0.44 Z-score*s; experienced, 0.53 ± 0.20 Z-score*s; paired t test, $p = 0.48$), or *Mecp2*^{HET} mice ($n = 8$; naive, 1.20 ± 0.31 Z-score*s; experienced, 1.03 ± 0.34 Z-score*s; paired t test, $p = 0.22$).

(Pizzorusso et al., 2002; Carulli et al., 2010; de Vivo et al., 2013; Donato et al., 2013; Happel et al., 2014; Hou et al., 2017; Cisneros-Franco and de Villers-Sidani, 2019; reviewed in Rupert and Shea, 2022). This was accompanied by a lack of the disinhibitory plasticity found in the auditory cortex WT mice after exposure to pups (Lau et al., 2020). Several manipulations that ameliorated PV and PNN overexpression in *Mecp2*^{HET} subjects led to a resumption of behavior and partial restoration of the neural disinhibitory response (Krishnan et al., 2017; Lau et al., 2020). Here, we present evidence that deletion of *Mecp2* selectively in PVins is sufficient to recreate many aspects of the neuropathology linked to the behavioral learning deficits that we observe in nonconditional, mosaic *Mecp2*^{HET} mutants. Importantly, just as in *Mecp2*^{HET} mice, the behavioral impairment could not be explained by gross locomotor deficits because there were no significant differences between wild types and mutants in mean velocity for any of the Cre lines.

Although our data emphasize the central importance of auditory cortical responses for pup retrieval, there are certainly other factors and brain regions that are important, including arousal state, oxytocin, and olfaction (Moreno et al., 2018). For example, pup retrieval is a multisensory behavior that jointly requires sound and smell (Cohen et al., 2011; Wang and Storm, 2011; Weiss et al., 2011; Fraser and Shah, 2014; Nowlan et al., 2022). Interestingly, when pup odor is delivered to the nose of either a dam or a maternally experienced surrogate, auditory cortical responses to sound, including pup calls, are modulated. Previously, we submitted an article to a preprint server in which we propose that this integration is accomplished via a pathway from pup-odor-responsive neurons in the basal amygdala to the auditory cortex (Nowlan et al., 2022). The implication of this is that acquisition and performance of pup retrieval involves multiple brain regions and stimuli. The odor-responsive input to the auditory cortex is especially interesting because it may be a mechanism for exposure to sensory

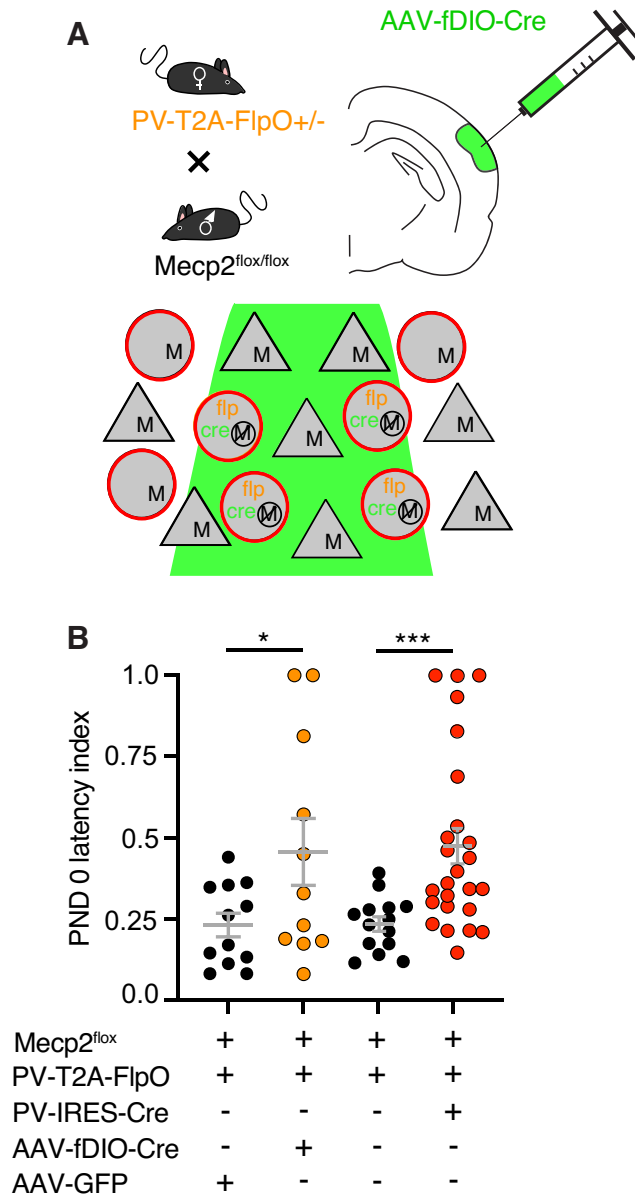


Figure 7. Acquisition of pup retrieval is delayed by adult loss of *Mecp2* in auditory cortex PVins. **A**, Schematic depiction of our experimental strategy. Mice carrying Flp recombinase after a T2A site in PV neurons were crossed with *Mecp2*^{flox} mice. Offspring mice positive for both alleles were injected with an AAV driving the expression of either Flp-dependent (fDIO) Cre or GFP. The consequence of injecting fDIO-Cre is the deletion of *Mecp2* from PV neurons at the time and location of our choosing, in this case, the auditory cortex of young adult mice, thereby deleting *Mecp2* in PVins at the injection site. **B**, Swarm plot comparing retrieval latencies for control subjects that were injected with AAV-GFP (left, black points) to those for subjects that were injected with AAV-fDIO-Cre (orange points). For direct comparison, prior data from PV-*Mecp2* WT (right, black points) and PV-*Mecp2* mutant (red points) are also provided. A one-way ANOVA of all groups revealed significant differences among them ($F = 5.02$, $p < 0.01$). Retrieval latencies were significantly longer in mice injected with fDIO-Cre compared with control mice injected with AAV-GFP ($n = 12$ controls, latency, 0.230 ± 0.04 ; $n = 12$ mutants, latency, 0.381 ± 0.08 ; Sidak's test, $*p < 0.05$).

characteristics of pups to trigger maternal experience-induced plasticity.

PVins have a disproportionate role in early establishment of retrieval behavior

Numerically speaking, cortical PVins make up a small population of neurons (accounting for $\sim 10\%$ of cortical neurons), yet

they can powerfully affect neural activity (Cardin, 2018). Indeed, we compared the effects of deleting *Mecp2* in PVins only with deleting it in two other major classes of cortical inhibitory neurons, SST and VIP neurons. These populations are slightly less numerous than PVins but are of the same order of magnitude. We found no detectable effect on retrieval performance of selectively deleting *Mecp2* in SSTins or VIPins. This points to a specific function during retrieval for PV neurons, among all inhibitory subtypes, that makes the brain especially vulnerable to their loss of *Mecp2*. As all the interneuron types interact in the cortical circuit, it is somewhat surprising to find such a specific behavioral effect from loss of *Mecp2* in only one type. However, this is not unprecedented, as loss of *Mecp2* in PV and SST neurons exhibit largely nonoverlapping subsets of the known characteristics of unconditional *Mecp2* knockouts (Ito-Ishida et al., 2015). Mice lacking *Mecp2* in VIP neurons have their own distinct characteristics such as differences in state-dependent brain activity and certain behaviors (Mossner et al., 2020). In any case, although it is reasonable to expect that different interneuron classes interact, it's important to note that their synaptic targets and timing of activity relative to behavior may orthogonalize their contributions to network activity in some circumstances.

Moreover, the admittedly short delay in the emergence of retrieval from PVins was no stronger or longer in mice that lacked *Mecp2* in homeobox protein box (Emx1) neurons, which constitute $\sim 88\%$ of cortical neuron. This again suggests that the much smaller PVin population plays a specific and disproportionately large role in auditory cortical plasticity. Notably, in both PVin and Emx1 populations, removing *Mecp2* caused only a delayed emergence of retrieval behavior, not the sustained deficit we observed in nonconditional, mosaic *Mecp2*^{het}. This suggests that *Mecp2* in PVin neurons and Emx1 neurons each have an obligatory role in the early initiation of auditory cortical plasticity, but not necessarily in its subsequent maintenance. Yet, complete *Mecp2* deletion in either PVin or Emx1 neurons is less potent than mosaic absence of *Mecp2* among all cell-type populations. This suggests that compensatory mechanisms involving nontargeted cell types attenuate the effects of deleting *Mecp2* in only one cell type. Based on the results of deleting *Mecp2* in PVins during early adulthood, such compensatory mechanisms do not involve developmental processes. Moreover, suppression of typical expression patterns of PNNs acutely, just before introduction of pups, was sufficient to improve behavior within 5 d, despite any changes in the preceding developmental trajectory. The four lines also differed considerably in their baseline behavioral variability, but they should not be directly compared with one another. We find that there can be substantial differences in this behavior among wild types of different lines, depending on genetic background. The only fair comparison is between wild types and mutants of the same line, which is why we use littermate controls.

Relationship of behavior to expression patterns and neurophysiology in PVins

PVin-specific deletion of *Mecp2* caused a very similar upregulation in PV and PNNs to that seen in mosaic *Mecp2*^{het} mutants (Krishnan et al., 2017). However, unlike *Mecp2*^{het} mice, the upregulation was a mix of transient and persistent increases. Specifically, PV-*Mecp2* mutants exhibited a persistent increase in staining intensity of PV protein, yet the increase in staining intensity of PNNs present on P1 subsided by P5. It is possible that the failure to sustain high levels of PNN staining limits the duration of the disruption of behavior in PV-*Mecp2* mutants. It is worth noting that because the changes in counts of PVins and

associated structures are so rapid (within 1–2 d), these changes very likely result from a change in expression intensity relative to our detection threshold, not a change in the absolute number of PVin cells themselves (i.e., cell-type identity is unlikely to change over such a short time course).

Our prior work suggested that PNN expression is closely related to retrieval performance; not only were expression and performance correlated, but the administration of chondroitinase to dissolve PNNs in the auditory cortex actually improved behavior in *Mecp2*^{het} (Krishnan et al., 2017). We therefore hypothesize that the long-term establishment of well-developed PNNs in the auditory cortex is a crucial barrier to the cortical plasticity underlying pup retrieval learning. Interestingly, deletion of *Mecp2* in PVins, although sufficient to establish more mature PNNs, is insufficient to sustain them. This implies that PNNs, despite preferentially surrounding PVins, are influenced by cell-autonomous and non-cell-autonomous processes on distinct timescales. In light of this, it will be interesting in future studies to see whether deletion of *Mecp2* in *Emx1* neurons also lead to increased PNN expression at PV synapses, that is, through a non-cell-autonomous mechanism.

Our past work also revealed that maternal experience triggers disinhibited activity in the auditory cortex of WT females. In WTs this disinhibition was mediated by PVins but was abolished in PV-*Mecp2* mutants (Lau et al., 2020). Here, we find that in PV-*Mecp2* mutants, PVins also do not decrease their stimulus-driven activity after the female acquires experience caring for pups. Because subjects in electrophysiology experiments were recorded after P6, and subjects in fiber photometry experiments were imaged through P5, the prevention of auditory cortical disinhibition outlasted the transient behavioral and molecular effects of *Mecp2* deletion in PVins.

In addition to regulating plasticity, *Mecp2* affects other aspects of cortical function. For example, despite the lack of effect here on maternal retrieval, it is important for maintaining normal activity patterns and behavior in other classes of cortical interneurons, including SSTins and VIPins (Ito-Ishida et al., 2015; Mossner et al., 2020). Loss of *Mecp2* function in all cortical interneurons, or even only in VIP interneurons specifically, leads to abnormal local field potential oscillations and disrupts the influence of the cortical state on the firing of individual neurons (Mossner et al., 2020). These phenotypes may reflect disruption of the balance between excitation and inhibition at the network level (Calfa et al., 2011; Banerjee et al., 2016; Li, 2022) and may also be a contributing factor to the susceptibility of *Mecp2* mutants to seizures (Dolce et al., 2013). Our understanding, as a field, of different contributions of inhibitory cell types to network activity and behavior, even apart from *Mecp2*, is still incomplete.

Deletion of *Mecp2* in PVins likely affects behavior by an acute and cell-autonomous mechanism

Importantly, our experiments with PV-specific *Mecp2* knockout removed *Mecp2* early in development and from all PV-expressing neurons throughout the brain. To bring greater spatiotemporal specificity to our manipulation, we adopted an intersectional strategy that required both Flp and Cre recombinases to remove *Mecp2*, allowing us to manipulate only PVins in the auditory cortex and only in adulthood. We found that this also produced a transient delay in pup retrieval, establishing that the plasticity mechanisms that support that behavior also acutely require *Mecp2* in adulthood rather than during development alone. This observation argues in favor of the likelihood that the transient behavioral disruption is a cell-autonomous consequence of loss

of *Mecp2* in PVins of the auditory cortex because those are the same cells that are the effectors of the circuit disruption.

Mecp2 and social behavior

Our study is not the first to show that loss of function of *Mecp2* leads to impaired social behavior. Indeed, early studies in mice reported that *Mecp2* mutants have altered social interactions, an attribute they share with humans who have Rett syndrome (Zoghbi, 2005; Moretti et al., 2006). However, there are divergent data on whether disabling *Mecp2* decreases (Gemelli et al., 2006; De Filippis et al., 2010) or increases (Pearson et al., 2012) sociability. The gene interacts differently with social behavior depending on the affected cell type. For example, loss of *Mecp2* in peripheral somatosensory neurons apparently interferes with social interaction by rendering mice hypersensitive and averse to gentle mechanosensory stimulation (Orefice et al., 2016, 2019). *Mecp2* expression is also crucial in the medial prefrontal cortex for discrimination of social partners by neuronal ensembles (Xu et al., 2022).

Implications and future directions

A number of questions remain that should be the focus of future work. First, although our optical and electrical recordings from the auditory cortex were performed in awake animals, it is not yet known how the disinhibition we observe interacts with ongoing activity in freely behaving mice that are performing pup retrieval. PVins are important to the phenotype of *Mecp2*^{het} mice, and they can modulate cortical activity from the single-unit level up to more widespread features of brain state (Cardin, 2018), including gamma oscillations (Cardin et al., 2009; Sohal et al., 2009). Recording from actively retrieving mice may reveal unappreciated dynamic influences such as locomotor activity and arousal that may be mediated by PVins (Nelson et al., 2013; Schneider et al., 2014; Henschke et al., 2021). Second, the relationship between PVin activity and construction of PNNs is not well understood. An interesting goal for future work will be to ascertain the relationship between PNNs and PVin activity and how they are affected by the activity of other cell types and on what time scale. Third, these questions about cell-autonomous and noncell-autonomous influences of *Mecp2* will be enlightened by targeted recordings from neurons that are individually identified as *Mecp2*⁺ and *Mecp2*⁻ in mosaic *Mecp2*^{het} mice.

References

- Amir RE, Van den Veyver IB, Wan M, Tran CQ, Francke U, Zoghbi HY (1999) Rett syndrome is caused by mutations in X-linked MECP2, encoding methyl-CpG-binding protein 2. *Nat Genet* 23:185–188.
- Banerjee A, Rikhye RV, Breton-Provencher V, Tang X, Li C, Li K, Runyan CA, Fu Z, Jaenisch R, Sur M (2016) Jointly reduced inhibition and excitation underlies circuit-wide changes in cortical processing in Rett syndrome. *Proc Natl Acad Sci U S A* 113:E7287–E7296.
- Bashina VM, Simashkova NV, Grachev VV, Gorbachevskaya NL (2002) Speech and motor disturbances in Rett syndrome. *Neurosci Behav Physiol* 32:323–327.
- Braunschweig D, Simcox T, Samaco RC, LaSalle JM (2004) X-Chromosome inactivation ratios affect wild-type MeCP2 expression within mosaic Rett syndrome and *Mecp2*^{-/+} mouse brain. *Hum Mol Genet* 13:1275–1286.
- Briata P, Di Blas E, Gulisano M, Mallamaci A, Iannone R, Boncinelli E, Corte G (1996) EMX1 homeoprotein is expressed in cell nuclei of the developing cerebral cortex and in the axons of the olfactory sensory neurons. *Mech Dev* 57:169–180.
- Calfa G, Hablitz JJ, Pozzo-Miller L (2011) Network hyperexcitability in hippocampal slices from *Mecp2* mutant mice revealed by voltage-sensitive dye imaging. *J Neurophysiol* 105:1768–1784.

- Carcea I, et al. (2021) Oxytocin neurons enable social transmission of maternal behaviour. *Nature* 596:553–557.
- Cardin JA (2018) Inhibitory interneurons regulate temporal precision and correlations in cortical circuits. *Trends Neurosci* 41:689–700.
- Cardin JA, Carlén M, Meletis K, Knoblich U, Zhang F, Deisseroth K, Tsai LH, Moore CI (2009) Driving fast-spiking cells induces gamma rhythm and controls sensory responses. *Nature* 459:663–667.
- Carulli D, Pizzorusso T, Kwok JC, Putignano E, Poli A, Forostyak S, Andrews MR, Deepa SS, Glant TT, Fawcett JW (2010) Animals lacking link protein have attenuated perineuronal nets and persistent plasticity. *Brain* 133:2331–2347.
- Cazakoff BN, Lau BY, Crump KL, Demmer HS, Shea SD (2014) Broadly tuned and respiration-independent inhibition in the olfactory bulb of awake mice. *Nat Neurosci* 17:569–576.
- Chao HT, Zoghbi HY, Rosenmund C (2007) MeCP2 controls excitatory synaptic strength by regulating glutamatergic synapse number. *Neuron* 56:58–65.
- Chao HT, Chen H, Samaco RC, Xue M, Chahrour M, Yoo J, Neul JL, Gong S, Lu HC, Heintz N, Ekker M, Rubenstein JL, Noebels JL, Rosenmund C, Zoghbi HY (2010) Dysfunction in GABA signalling mediates autism-like stereotypies and Rett syndrome phenotypes. *Nature* 468:263–269.
- Chen RZ, Akbarian S, Tudor M, Jaenisch R (2001) Deficiency of methyl-CpG binding protein-2 in CNS neurons results in a Rett-like phenotype in mice. *Nat Genet* 27:327–331.
- Cisneros-Franco JM, de Villers-Sidani E (2019) Reactivation of critical period plasticity in adult auditory cortex through chemogenetic silencing of parvalbumin-positive interneurons. *Proc Natl Acad Sci U S A* 116:26329–26331.
- Cohen L, Mizrahi A (2015) Plasticity during motherhood: changes in excitatory and inhibitory layer 2/3 neurons in auditory cortex. *J Neurosci* 35:1806–1815.
- Cohen L, Rothschild G, Mizrahi A (2011) Multisensory integration of natural odors and sounds in the auditory cortex. *Neuron* 72:357–369.
- De Filippis B, Ricceri L, Laviola G (2010) Early postnatal behavioral changes in the Mecp2-308 truncation mouse model of Rett syndrome. *Genes Brain Behav* 9:213–223.
- Deng JV, Rodriguiz RM, Hutchinson AN, Kim IH, Wetsel WC, West AE (2010) MeCP2 in the nucleus accumbens contributes to neural and behavioral responses to psychostimulants. *Nat Neurosci* 13:1128–1136.
- Deng JV, Wan Y, Wang X, Cohen S, Wetsel WC, Greenberg ME, Kenny PJ, Calakos N, West AE (2014) MeCP2 phosphorylation limits psychostimulant-induced behavioral and neuronal plasticity. *J Neurosci* 34:4519–4527.
- de Vivo L, Landi S, Panniello M, Baroncelli L, Chierzi S, Mariotti L, Spolidoro M, Pizzorusso T, Maffei L, Ratto GM (2013) Extracellular matrix inhibits structural and functional plasticity of dendritic spines in the adult visual cortex. *Nat Commun* 4:1484.
- Dolce A, Ben-Zeev B, Naidu S, Kossoff EH (2013) Rett syndrome and epilepsy: an update for child neurologists. *Pediatr Neurol* 48:337–345.
- Donato F, Rompani SB, Caroni P (2013) Parvalbumin-expressing basket-cell network plasticity induced by experience regulates adult learning. *Nature* 504:272–276.
- Dvorkin R, Shea SD (2022) Precise and pervasive phasic bursting in locus coeruleus during maternal behavior in mice. *J Neurosci* 42:2986–2999.
- Ehret G, Koch M, Haack B, Markl H (1987) Sex and parental experience determine the onset of an instinctive behavior in mice. *Naturwissenschaften* 74:47.
- Fraser EJ, Shah NM (2014) Complex chemosensory control of female reproductive behaviors. *PLoS One* 9:e90368.
- Galindo-Leon EE, Lin FG, Liu RC (2009) Inhibitory plasticity in a lateral band improves cortical detection of natural vocalizations. *Neuron* 62:705–716.
- Gemelli T, Berton O, Nelson ED, Perrotti LI, Jaenisch R, Monteggia LM (2006) Postnatal loss of methyl-CpG binding protein 2 in the forebrain is sufficient to mediate behavioral aspects of Rett syndrome in mice. *Biol Psychiatry* 59:468–476.
- Glaze DG (2005) Neurophysiology of Rett syndrome. *J Child Neurol* 20:740–746.
- Gulmez Karaca K, Brito DVC, Zeuch B, Oliveira AMM (2018) Adult hippocampal MeCP2 preserves the genomic responsiveness to learning required for long-term memory formation. *Neurobiol Learn Mem* 149:84–97.
- Guy J, Hendrich B, Holmes M, Martin JE, Bird A (2001) A mouse Mecp2-null mutation causes neurological symptoms that mimic Rett syndrome. *Nat Genet* 27:322–326.
- Happel MF, Niekisch H, Castiblanco Rivera LL, Ohl FW, Deliano M, Frischknecht R (2014) Enhanced cognitive flexibility in reversal learning induced by removal of the extracellular matrix in auditory cortex. *Proc Natl Acad Sci U S A* 111:2800–2805.
- He LJ, Liu N, Cheng TL, Chen XJ, Li YD, Shu YS, Qiu ZL, Zhang XH (2014) Conditional deletion of Mecp2 in parvalbumin-expressing GABAergic cells results in the absence of critical period plasticity. *Nat Commun* 5:5036.
- Henschke JU, Price AT, Pakan JMP (2021) Enhanced modulation of cell-type specific neuronal responses in mouse dorsal auditory field during locomotion. *Cell Calcium* 96:102390.
- Hou X, Yoshioka N, Tsukano H, Sakai A, Miyata S, Watanabe Y, Yanagawa Y, Sakimura K, Takeuchi K, Kitagawa H, Hensch TK, Shibuki K, Igarashi M, Sugiyama S (2017) Chondroitin sulfate is required for onset and offset of critical period plasticity in visual cortex. *Sci Rep* 7:12646.
- Ito-Ishida A, Ure K, Chen H, Swann JW, Zoghbi HY (2015) Loss of MeCP2 in parvalbumin- and somatostatin-expressing neurons in mice leads to distinct Rett syndrome-like phenotypes. *Neuron* 88:651–658.
- Krishnan K, Wang BS, Lu J, Wang L, Maffei A, Cang J, Huang ZJ (2015) MeCP2 regulates the timing of critical period plasticity that shapes functional connectivity in primary visual cortex. *Proc Natl Acad Sci U S A* 112:E4782–4791.
- Krishnan K, Lau BY, Ewall G, Huang ZJ, Shea SD (2017) MECP2 regulates cortical plasticity underlying a learned behaviour in adult female mice. *Nat Commun* 8:14077.
- Lau BYB, Krishnan K, Huang ZJ, Shea SD (2020) Maternal experience-dependent cortical plasticity in mice is circuit- and stimulus-specific and requires MECP2. *J Neurosci* 40:1514–1526.
- Li W (2022) Excitation and inhibition imbalance in Rett syndrome. *Front Neurosci* 16:825063.
- Lin FG, Galindo-Leon EE, Ivanova TN, Mappus RC, Liu RC (2013) A role for maternal physiological state in preserving auditory cortical plasticity for salient infant calls. *Neuroscience* 247:102–116.
- Liu RC, Schreiner CE (2007) Auditory cortical detection and discrimination correlates with communicative significance. *PLoS Biol* 5:e173.
- Marlin BJ, Mitre M, D'Amour JA, Chao MV, Froemke RC (2015) Oxytocin enables maternal behaviour by balancing cortical inhibition. *Nature* 520:499–504.
- Mathis A, Mamidanna P, Cury KM, Abe T, Murthy VN, Mathis MW, Bethge M (2018) DeepLabCut: markerless pose estimation of user-defined body parts with deep learning. *Nat Neurosci* 21:1281–1289.
- McGraw CM, Samaco RC, Zoghbi HY (2011) Adult neural function requires MeCP2. *Science* 333:186.
- Meng X, Wang W, Lu H, He LJ, Chen W, Chao ES, Fiorotto ML, Tang B, Herrera JA, Seymour ML, Neul JL, Pereira FA, Tang J, Xue M, Zoghbi HY (2016) Manipulations of MeCP2 in glutamatergic neurons highlight their contributions to Rett and other neurological disorders. *Elife* 5:e14199.
- Moreno A, Gumaste A, Adams GK, Chong KK, Nguyen M, Shepard KN, Liu RC (2018) Familiarity with social sounds alters c-Fos expression in auditory cortex and interacts with estradiol in locus coeruleus. *Hear Res* 366:38–49.
- Moretti P, Levenson JM, Battaglia F, Atkinson R, Teague R, Antalffy B, Armstrong D, Arancio O, Sweatt JD, Zoghbi HY (2006) Learning and memory and synaptic plasticity are impaired in a mouse model of Rett syndrome. *J Neurosci* 26:319–327.
- Mossner JM, Batista-Brito R, Pant R, Cardin JA (2020) Developmental loss of MeCP2 from VIP interneurons impairs cortical function and behavior. *Elife* 9:e55639.
- Na ES, Nelson ED, Kavalali ET, Monteggia LM (2013) The impact of MeCP2 loss- or gain-of-function on synaptic plasticity. *Neuropsychopharmacology* 38:212–219.
- Nelson A, Schneider DM, Takatoh J, Sakurai K, Wang F, Mooney R (2013) A circuit for motor cortical modulation of auditory cortical activity. *J Neurosci* 33:14342–14353.
- Noutel J, Hong YK, Leu B, Kang E, Chen C (2011) Experience-dependent retinogeniculate synapse remodeling is abnormal in MeCP2-deficient mice. *Neuron* 70:35–42.

- Nowlan AC, Kelehan C, Shea SD (2022) Multisensory integration of social signals by a pathway from the basal amygdala to the auditory cortex in maternal mice. *bioRxiv* 480854. <https://doi.org/10.1101/2022.02.17.480854>.
- Orefice LL, Zimmerman AL, Chirila AM, Sleboda SJ, Head JP, Ginty DD (2016) Peripheral mechanosensory neuron dysfunction underlies tactile and behavioral deficits in mouse models of ASDs. *Cell* 166:299–313.
- Orefice LL, Mosko JR, Morency DT, Wells MF, Tasnim A, Mozeika SM, Ye M, Chirila AM, Emanuel AJ, Rankin G, Fame RM, Lehtinen MK, Feng G, Ginty DD (2019) Targeting peripheral somatosensory neurons to improve tactile-related phenotypes in ASD models. *Cell* 178:867–886.e24.
- Oswald AM, Reyes AD (2011) Development of inhibitory timescales in auditory cortex. *Cereb Cortex* 21:1351–1361.
- Pearson BL, Defensor EB, Pobbe RL, Yamamoto LH, Bolivar VJ, Blanchard DC, Blanchard RJ (2012) Mecp2 truncation in male mice promotes affiliative social behavior. *Behav Genet* 42:299–312.
- Pizzorusso T, Medini P, Berardi N, Chierzi S, Fawcett JW, Maffei L (2002) Reactivation of ocular dominance plasticity in the adult visual cortex. *Science* 298:1248–1251.
- Rosenblatt JS (1967) Nonhormonal basis of maternal behavior in the rat. *Science* 156:1512–1514.
- Rupert DD, Shea SD (2022) Parvalbumin-positive interneurons regulate cortical sensory plasticity in adulthood and development through shared mechanisms. *Front Neural Circuits* 16:886629.
- Samaco RC, Fryer JD, Ren J, Fyffe S, Chao HT, Sun Y, Greer JJ, Zoghbi HY, Neul JL (2008) A partial loss of function allele of methyl-CpG-binding protein 2 predicts a human neurodevelopmental syndrome. *Hum Mol Genet* 17:1718–1727.
- Schneider DM, Nelson A, Mooney R (2014) A synaptic and circuit basis for corollary discharge in the auditory cortex. *Nature* 513:189–194.
- Sewell GD (1970) Ultrasonic communication in rodents. *Nature* 227:410.
- Sohal VS, Zhang F, Yizhar O, Deisseroth K (2009) Parvalbumin neurons and gamma rhythms enhance cortical circuit performance. *Nature* 459:698–702.
- Tai DJ, Liu YC, Hsu WL, Ma YL, Cheng SJ, Liu SY, Lee EH (2016) MeCP2 SUMOylation rescues Mecp2-mutant-induced behavioural deficits in a mouse model of Rett syndrome. *Nat Commun* 7:10552.
- Van den Veyver IB, Zoghbi HY (2000) Methyl-CpG-binding protein 2 mutations in Rett syndrome. *Curr Opin Genet Dev* 10:275–279.
- Wang Z, Storm DR (2011) Maternal behavior is impaired in female mice lacking type 3 adenylyl cyclase. *Neuropsychopharmacology* 36:772–781.
- Weiss J, Pyrski M, Jacobi E, Bufe B, Willnecker V, Schick B, Zizzari P, Gossage SJ, Greer CA, Leinders-Zufall T, Woods CG, Wood JN, Zufall F (2011) Loss-of-function mutations in sodium channel Nav1.7 cause anosmia. *Nature* 472:186–190.
- Wu GK, Arbuckle R, Liu BH, Tao HW, Zhang LI (2008) Lateral sharpening of cortical frequency tuning by approximately balanced inhibition. *Neuron* 58:132–143.
- Xu P, Yue Y, Su J, Sun X, Du H, Liu Z, Simha R, Zhou J, Zeng C, Lu H (2022) Pattern decorrelation in the mouse medial prefrontal cortex enables social preference and requires MeCP2. *Nat Commun* 13:3899.
- Zoghbi HY (2005) MeCP2 dysfunction in humans and mice. *J Child Neurol* 20:736–740.